BRNO UNIVERSITY OF TECHNOLOGY

VYSOKÉ UČENÍ TECHNICKÉ V BRNĚ

FACULTY OF ELECTRICAL ENGINEERING AND COMMUNICATION

FAKULTA ELEKTROTECHNIKY
A KOMUNIKAČNÍCH TECHNOLOGIÍ

DEPARTMENT OF ELECTRICAL POWER ENGINEERING

ÚSTAV ELEKTROENERGETIKY

DETERMINATION OF NUCLEAR REACTIONS' MICROSCOPIC CROSS-SECTIONS USING AN ACCELERATOR-DRIVEN NEUTRON SOURCE

URČOVÁNÍ MIKROSKOPICKÝCH ÚČINNÝCH PRŮŘEZŮ JADERNÝCH REAKCÍ POMOCÍ URYCHLOVAČEM ŘÍZENÉHO NEUTRONOVÉHO ZDROJE

MASTER'S THESIS
DIPLOMOVÁ PRÁCE

AUTHOR
AUTOR PRÁCE

Bc. Vendula Filová

SUPERVISOR
VEDOUCÍ PRÁCE

Ing. Dušan Král

BRNO 2022

Master's Thesis

Master's study program **Electrical Power Engineering**

Department of Electrical Power Engineering

Student:	Bc. Vendula Filová	*ID:*	184200
Year of study:	2	*Academic year:*	2021/22

TITLE OF THESIS:

Determination of nuclear reactions' microscopic cross-sections using an accelerator-driven neutron source

INSTRUCTION:

1. Perform research on neutron sources, and their basic classification according to their use and parameters.

2. Research and description of methods of measurement of microscopic cross-sections of nuclear reactions using neutron sources with a focus on quasi-mono-energetic neutron sources.

3. Process and evaluate experimental data from the Li target station of the U-120M cyclotron accelerator for indium samples.

4. As a part of the data evaluation, perform a Monte Carlo simulation of the experiment.

5. Compare measured data with the EXFOR database and the validated data from the ENDF databases.

RECOMMENDED LITERATURE:

DEBERTIN, Klaus; HELMER, Richard G. Gamma-and X-ray spectrometry with semiconductor detectors. 1988.

MAJERLE, Mitja, et al. Peak neutron production from the 7Li (p, n) reaction in the 20-35 MeV range. In: EPJ Web of Conferences. EDP Sciences, 2020. p. 20010.

MAJERLE, Mitja, et al. natCu and natV cross-sections measured by quasi-monoenergetic neutrons from p+ 7Li reaction in the energy range of 18–34 MeV. In: EPJ Web of Conferences. EDP Sciences, 2017. p. 09019.

ŠIMEČKOVÁ, Eva, et al. The activation cross section measurements of proton-induced reactions on Li and Ta in the energy region 12.5–34 MeV. Nuclear Physics A, 2021, 1016: 122310.

CHUDOBA, Petr, et al. Activation Measurements of Cross Sections for Ground and Isomeric States Production in Neutron Threshold Reactions on Y and Au. Nuclear Science and Engineering, 2018, 191.2: 150-160.

MAJERLE, Mitja, et al. Cross sections measured by quasi-monoenergetic neutrons. Radiation protection dosimetry, 2018, 180.1-4: 386-390.

Date of project specification:	7.2.2022	*Deadline for submission:*	24.5.2022

Supervisor:	Ing. Dušan Král
Consultant:	doc. Ing. Karel Katovský, Ph.D.

prof. Ing. Petr Toman, Ph.D.
Chair of study program board

ABSTRACT

The thesis focuses on a determination of microscopic cross-sections of interactions of neutrons with indium. The theoretical part of the thesis summarizes neutron sources used in science and industry, describes principles of their function and presents examples of their usage. The practical part describes the evaluation procedure of microscopic cross-sections, including individual corrections. Data from three experiments were evaluated, neutrons were produced via interaction of proton with the thin lithium target. Sandwiches of various foils were irradiated by these quasi mono-energetic neutrons, and products of interactions were measured via γ spectroscopy. Resultant microscopic cross-sections are compared to data from libraries of evaluated data and with values from the EXFOR library.

KEYWORDS

cross-section, gamma spectroscopy, HPGe, neutron, neutron source, quasi-monoenergetic neutron spectrum

ABSTRAKT

Tato práce se věnuje určení mikroskopických účinných průřezů interakcí neutronů s indiem. Teoretická část shrnuje neutronové zdroje používané ve vědě i průmyslu, popisuje princip jejich fungování a představuje příklady jejich aplikací. Praktická část obsahuje postup vyhodnocování velikostí účinných průřezů včetně jednotlivých provedených korekcí. Byly vyhodnocována data celkem ze tří experimentů, při kterých byly produkovány neutrony interakcí protonů s tenkým lithiovým terčem. Kvazi monoenergetickým neutronům byly vystaveny sendviče folií včetně foile z india, produkty interakcí byly měřeny pomocí γ spektrometrie. Výsledné mikroskopické účinné průřezy jsou porovnány s daty z knihoven evaluovaných dat a z knihovny EXFOR.

KLÍČOVÁ SLOVA

gamma spetroskopie, HPGe, kvazi-monoenergetické neutronové spektrum, neutron, zdroj neutronů, účinný průřez

ROZŠÍŘENÝ ABSTRAKT

Neutrony jsou spolu s protony subatomární částice. Vyznačují se tím, že na rozdíl od protonů nemají elektrický náboj. To je výhodné pro velké množství aplikací, jelikož elektromagneticky neinteragují ani s atomovým obalem, ani s jeho jádrem. Této vlastnosti se využívá například při neutronovém zobrazování.

Pravděpodobnost, s jakou dojde k určité interakci neutronu s daným izotopem, se nazývá účinný průřez. Znalost účinných průřezů je nutná pro výzkum a vývoj například materiálů či radiofarmak. Dalším důvodem pro určování účinných průřezů může být fakt, že neutrony kvůli absenci elektrického náboje není možné detekovat přímo. Je třeba využít vhodného konverzního materiálu a účinné průřezy jednotlivých reakcí jsou jedním z aspektů jeho výběru.

Tématem této diplomové práce je určení mikroskopických účinných průřezů pro reakce kvazi monoenergetických neutronů produkovaných srážkou protonů s tenkým lithiovým terčem na indiu. Měření probíhala na cyklotronu v ÚJF Řež a byla provedena vedoucím této diplomové práce, Ing. Dušanem Králem. Jsou zpracovány výsledky celkem tří experimentů, probíhajících v letech 2018 a 2019.

Experimentální sestava byla tvořena zdrojem neutronů, tedy lithiovým terčem ostřelovaným protony. Energie protonů se lišila pro jednotlivé experimenty (20 MeV, 31.5 MeV a 35.5 MeV). Ozařovány byly sendvičově uspořádané folie z různých materiálů, jako například železo či vanad. Pro účely této práce budou zmiňovány pouze folie z přírodního india a zlata, kdy zlatá folie byla vždy umístěna jako poslední pro určení husoty neutronového toku. Folie byly po ukončení ozařování přemístěny ke HPGe detektorům za účelem měření gamma spekter.

Zpracování naměřených dat sestává z řady kroků. Nejprve je třeba vyhodnotit spektra naměřená HPGe detektory. K tomuto účelu byl využit program Deimos, vytvořený v ÚJV Řež. Tento program umožňuje proklady jednotlivých píků ve spektru a tím určení jejich plochy. Výstupní soubory z programu Deimos slouží jako vstupy pro software vyvinutý na UEEN. Ten slouží k určení produkčních rychlostí izotopů vznikajících při ozařování dané folie. Software provede všechny potřebné spektrometrické korekce, jejichž manuální aplikace by byla zdlouhavá a komplikovaná. Výstupem je excelový soubor obsahující vypočtené produkční rychlosti a jejich nejistoty.

Dále byly provedeny simulace experimentu pomocí kódu MCNP. Za tímto účelem byl použit model experimentální sestavy, jehož autorem je M. Majerle, působící v ÚJF Řež. Tento model byl upraven pro použití ve verzi MCNP6.2. Pomocí tally F4 byl sledován neutronový tok v buňkách folií india a zlata, který sloužil k výpočtu korekce na neutronové pozadí.

Dalším krokem byly simulace účinných průřezů pro reakce na jednotlivých izotopech folií, tedy ^{113}In, ^{115}In a ^{197}Au. Vyhodnocená data jsou zatížena velkým

množstvím nejistot. Ty mohou mít různé příčiny. Samotný způsob měření je ovlivněný účinností detektoru, dobou měření od konce ozařování, tloušťkou vzorku atd. Spektra produktů přeměny měřených radionuklidů mají v některých případech píky s velmi blízkou až totožnou energií, což komplikuje jejich vzájemné odlišení. Dalším zdrojem nejistoty je neutronové pozadí a způsob jeho odečtu. Výpočty jsou také závislé na použitých knihovnách jaderných dat.

Při přihlédnutí k velkému množství faktorů, které ovlivňují výsledky výpočtů je možné konstatovat, že naměřená data odpovídají referenčním hodnotám z knihoven evaluovaných dat. V případě dat, která se od referenčních hodnot vzdalují je popsán pravděpodobný důvod odchylky.

Přínosem práce je zejména vyhodnocení mikroskopických účinných průřezů pro oblasti energií, pro kterou prakticky neexistují experimentální data v knihovně EXFOR. Dalším přínosem je i ověření funkčnosti používaného softwaru pro vyhodnocování γ spekter.

Author's Declaration

Author:	Bc. Vendula Filová
Author's ID:	184200
Paper type:	Master's Thesis
Academic year:	2021/22
Topic:	Determination of nuclear reactions' microscopic cross-sections using an accelerator-driven neutron source

I declare that I have written this paper independently, under the guidance of the advisor and using exclusively the technical references and other sources of information cited in the paper and listed in the comprehensive bibliography at the end of the paper.

As the author, I furthermore declare that, with respect to the creation of this paper, I have not infringed any copyright or violated anyone's personal and/or ownership rights. In this context, I am fully aware of the consequences of breaking Regulation $\S\,11$ of the Copyright Act No. 121/2000 Coll. of the Czech Republic, as amended, and of any breach of rights related to intellectual property or introduced within amendments to relevant Acts such as the Intellectual Property Act or the Criminal Code, Act No. 40/2009 Coll. of the Czech Republic, Section 2, Head VI, Part 4.

Brno . . . . 　　　　　. . . . .

author's signature*

---

*The author signs only in the printed version.

ACKNOWLEDGEMENT

Contents

List of Figures

List of Tables

Introduction

"For the world is changing:" [1] the electrical energy consumption is rising[1] and the most common prediction is that the trend will not change in the following decades. The aim of the Paris agreement to keep the increase of the average temperature under 2 °C can be affected by the fact that even in 2020, 61 % of electricity worldwide came from fossil fuels [2]. In the aim of fulfilling the agreement, it is necessary to replace sources that are based on this type of fuel.

Neutrons can play an important role, especially since the EU proposed to label nuclear energy as a "green" source. Nuclear power plants are the most known method of use of neutrons because they are an essential part of ongoing fission reactions. However, that is only one of the possible neutron applications.

A atom nucleus consists of a proton and a neutron. The neutron is similar to the proton in the meaning of mass, but it has no electric charge. However, it has a magnetic moment. If it is not bounded in the nucleus, the neutron is unstable and decays with a half-life of 611 s.

Since neutrons are not charged particles, they can penetrate deep into the investigated matter. Neutron scattering, as a method of probing various materials, is advantageous in the sense that it is nondestructive. The great advantage of neutrons is also that they can distinguish between different isotopes of a single element. How neutrons scatter from light elements such as hydrogen or lithium enables to probe structures that would be invisible to x-rays. This can be used to increase the efficiency of renewable energy sources, i.e., in the development of lithium batteries or organic solar cells [3].

Neutrons also play a significant role in medicine. Research reactors worldwide are used to produce ^{99}Mo. This isotope is one of the possible products of ^{235}U fission. It decays to ^{99m}Tc, which is used for diagnostic imaging in hospitals worldwide. The reason to produce molybdenum is that its half-life is 66 hours, eleven times higher than for technetium. Another possibility is cancer treatment via so-called Boron Neutron Capture Therapy (BNCT), which benefits from the fact that boron absorbs neutrons easily. This leads to the release of an α particle. If boron fills the tumor cell, α rays can destroy it [4].

Neutrons can be helpful also in the exploration of the universe due to the production of ^{238}Pu, which is used as a power source in spacecrafts. The NASA Curiosity rover at Mars [5] searches for water under the planet's surface using neutron measurement. It is also a powerful tool in archaeology, due to the possibility of probing historical artifacts without direct contact, or in the fabrication of semiconductors

---

[1]According to [2] the consumption of electric energy was rising since 2009 except for 2020 when the demand fell (0.1 %) due to the global pandemic of COVID-19.

for an easy method of silicon doping. Explosive and hazardous materials can be investigated safely, also oil well logging or cargo screening is possible.

In the food industry, as well as in medicine, cosmetics, etc., it is advantageous to use the radioisotope as a source of γ rays for sterilization. This isotope is produced by the bombardment of natural cobalt by neutrons.

The above text shows that neutrons are a useful tool that should not be abandoned. For this purpose, it is necessary a network of neutron sources. However, the current situation is that a lot of research reactors will be shut down in the following years. To ensure that the demand for neutrons will be fulfilled, it is essential to come up with a proper strategy for replacing such important sources.

Many neutron applications require source compactness. For this reason, are very popular radioisotopic sources. There is a general attempt to replace these with sources based on neutron production through the interaction of accelerated particles with a target material. Commercially available neutron generators are strong competitors.

The theoretical part of this thesis aims to summarize the neutron sources that are available today or will be built in the near future. The thesis describes the process of neutron production via various reactions. Some of the most important projects focused on neutron production are also introduced.

The practical part is focused on the estimation of microscopic cross-sections of neutron interactions with nuclei of indium. The neutrons were produced via the interaction of protons with the lithium target. The results are compared with the evaluated data from nuclear data libraries.

Indium was chosen due to its large microscopic cross-sections for some of its interactions with neutrons and it is advantageous to search for its cross-sections in a region of higher energies.

1 Neutron sources

The neutron source is a device, which emits neutrons. Because of the unique parameters of neutrons, as was described in the introduction, they can be used in various fields of science, medicine, and industry. There are plenty of possibilities for their classification. For this thesis, neutron sources will be divided into several groups.

The sources from the first group described in the following paragraphs are those based on the natural radioactivity of the used isotope. From the nature of these sources, it is clear that they operate in a continuous mode and the spread of neutrons is isotropic. From the point of view of radiation protection, they are connected with hazardous quantities of radioactivity. They can also be sources of high γ-ray background. However, because of their compact dimensions, they can be easily shielded. The amount of radioisotope determines the power of the source, and the type of radioisotope influences its spectrum. These are the most widely used sources.

For other sources, it is characteristic that they can be switched off. That is a great advantage, leading to more convenient conditions from the radiation protection point of view. Usage of these sources also leads to a lesser level of background γ-rays compared to radioisotopic sources. Furthermore, the convenient choice of the combination of projectile and target can lead to the final directional neutron beam. The main disadvantage is the cost, which is significantly higher than in the case of the first group [6].

Neutrons can be produced in various ranges of energy. For easier classification, they are usually divided into energy groups. Quantities and ranges of these groups can differ according to the purpose of the selected group system. Ranges in Tab. 1.1 correspond to the general understanding.

Tab. 1.1: Neutron energy ranges.

Ultra cold neutrons	$< 1\,\mu eV$
Cold and very cold neutrons	1 μeV - 0.5 meV
Thermal neutrons	0.002 - 0.5 eV
Cadmium cut-off	0.5 eV
Epithermal neutrons	0.5 eV - 10 keV
Slow neutrons	< 0.3 eV
Fast neutrons	0.3 eV - 20 MeV
High energy neutrons	20 - 100 MeV
Relativistic neutrons	0.1 - 10 GeV
Ultrarelativistic neutrons	> 10 GeV

Most of the sources produce fast neutrons. On the contrary, it is most widely required to use thermal and cold neutrons, due to their characteristic interactions with matter. For this purpose, neutrons have to be properly moderated. The hydrogenous materials are the most effective neutron moderators. To reach the thermal region, water or polyethylene are used. For moderation up to the cold neutron energy region, solid methane or liquid hydrogen can be used [8].

The important property of each of the following neutron sources is its neutron spectrum. Its shape depends on the type of reaction that leads to the production of neutrons. We recognize the (quasi) monoenergetic, white, fission and spallation spectra, eventually their variances. Fig. 1.1 compares the shapes of fission, spallation (a), and quasi-monoenergetic (b) neutron spectra.

(a)   (b)
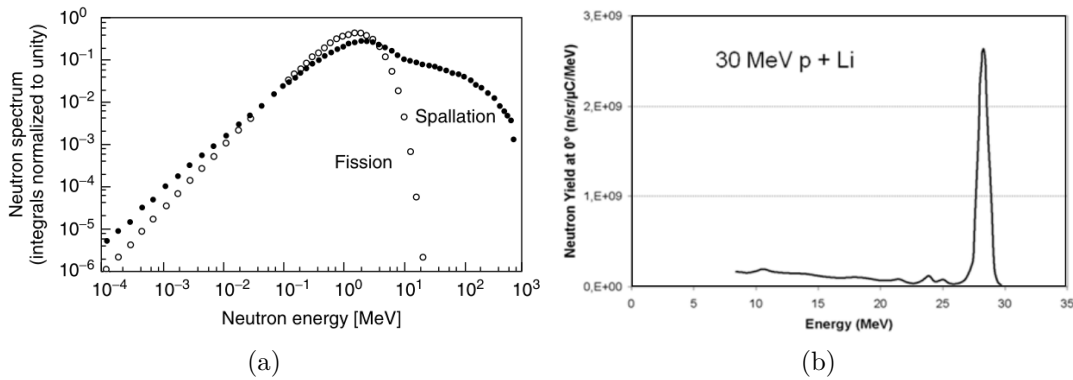
(a) Fission, spallation [9] and (b) quasi-monoenergetic [10] neutron spectra.

Fig. 1.1: The comparison of shapes of neutron spectra.

Especially in the case of large research facilities, it would be impossible to place all instruments near enough to the source. Various neutron beam guide lines (as in Fig. 1.2) can be used for this purpose. This is based on the principle of neutron mir-

Fig. 1.2: Neutron guides manufactured by S-DH [12].

ror reflection, which is fundamentally the same as the light reflection. The refractive index depends on the ability of the mirror material to scatter neutrons [11].

1.1 Radioisotopic sources

As was already mentioned, for this group of sources, the reason for the production of neutrons is the usage of an isotope that undergoes radioactive decay. They are used for startups of nuclear reactors, in material analysis, in science and education fields. Their compactness makes them suitable for industrial usage. These sources are made (double) encapsulated to avoid leakage (especially in the case of AmBe, which is in the form of powder). In the following paragraphs are introduced the most common kinds of such sources.

Figure 1.3 compares the normalized energy spectra of some of the neutron sources by their relative intensity.
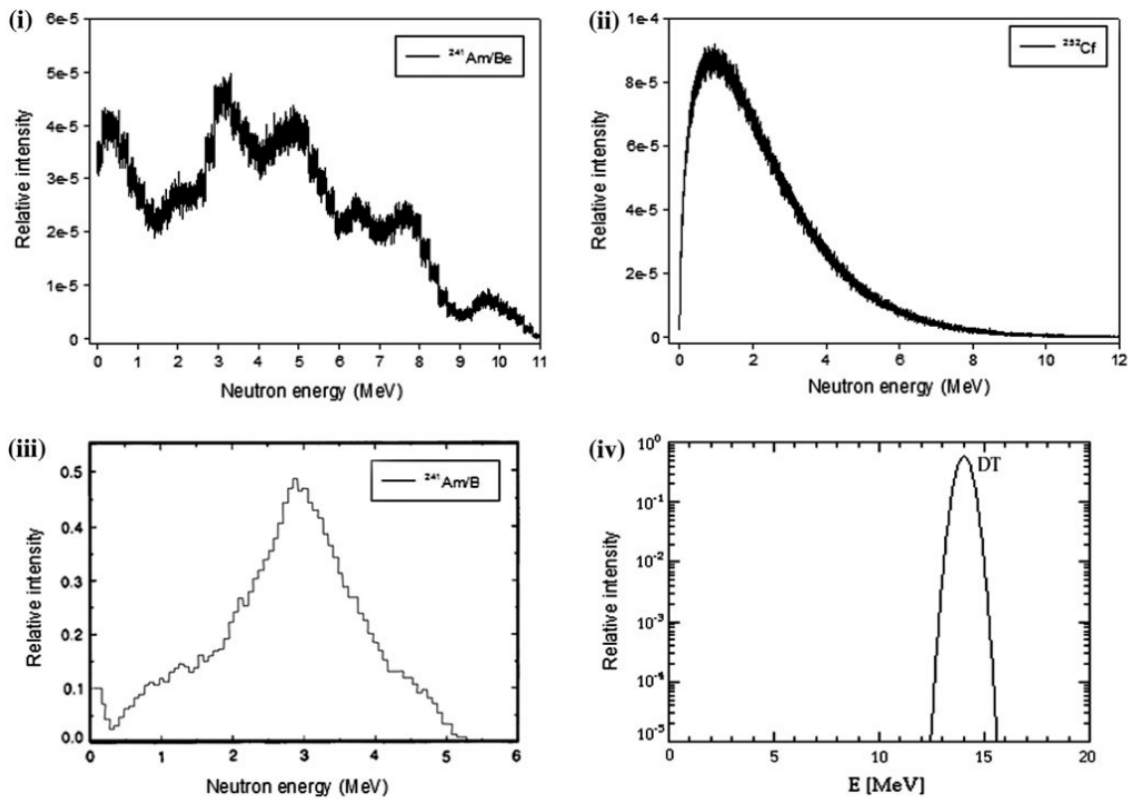
Fig. 1.3: Spectra of radioisotopic neutron sources (i) AmBe, (ii) ^{252}Cf, (iii) AmB, compared to (iv) neutron generator based on DT reaction according to [13].

1.1.1 Spontaneous fission

Isotopes with high mass numbers, such as ^{252}Cf can undergo spontaneous fission. These isotopes are mostly α radioactive and only about 3 % of the total decay are contributed by spontaneous fission. The energy of the released neutrons has a typical fission distribution, which can be described by Watt distribution, with an average energy value of 2.3 MeV for ^{252}Cf [14]. The neutron energy spectrum is shown in Fig. 1.3 (ii). The source has a relatively high neutron yield (see Tab. 1.2), however, the main disadvantage is its half-life, which is only 2.6 years [15]. This kind of source is suitable for usage in oil well logging, Portable Isotopic Neutron Spectroscopy System (PINS) - a method to inspect hazardous materials such as chemical weapons, and Prompt Gamma Neutron Activation Analysis (PGNAA), which is a method to determine the composition of the inspected material. These sources are usually encapsulated in stainless steel, zircaloy, etc. [16] In Fig. 1.4 is a visualization of a commercially available source.
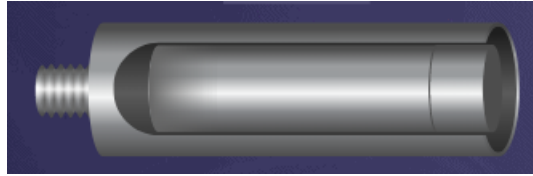
Fig. 1.4: The model of ^{252}Cf neutron source made by FTC company [16].

1.1.2 Neutron sources based on alpha emitters

In 1932, Chadwick announced the discovery of a new particle, called the neutron. The experiment he made was based on (α,n)[1] neutron source, specifically ^{210}Po^{9}Be [17]. The combination of a material of low atomic number (beryllium is the most commonly used material) with an isotope that emits α particles leads to the production of neutrons according to the equation:

$$^9\text{Be} +^4 \text{He} \rightarrow^{12} \text{C} +^1 \text{n} + \gamma, \tag{1.1}$$
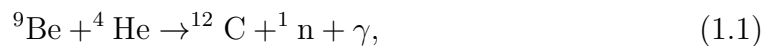
where γ with energy 4.43 MeV (the first excited state of ^{12}C [15]) can be released because the carbon nucleus can be left in an excited state. However, lithium, boron,

---

[1]There is a conventional notation for nuclear reactions. If the particle **p** impinges on the target nucleus **T**, the products of this interaction are the resultant nucleus **R** and the outgoing particle **o**. The whole process can be noted as T(p,o)R. If there are described various interactions that are invoked by particle **p** and outgoing particle **o**, it can be noted as (p,o).

carbon, fluorine, or oxygen can be used instead of beryllium, with a lower neutron yield [21].

At first, it was used the combination of beryllium with naturally occurring isotopes (^{210}Po or ^{226}Ra), but the neutron yield is low. ^{241}Am and ^{238}Pu are usually used as the α emitter. The AmBe source is standardized by International Organization for Standardization (ISO) [18]. The spectrum is continuous due to the character of the spectrum of the emitted α particles. Fig. 1.3 shows spectra of two sources, one uses beryllium and one uses boron. It is visible that the type of the neutron emitter influences the shape of the spectrum. The average neutron energy differs depending on the used α emitter. Tab. 1.2 shows neutron yields and mean neutron energies for some of these sources. In comparison to the ^{252}Cf source, neutron yields are significantly lower; on the other hand, their half-life and thus the stability is much higher.
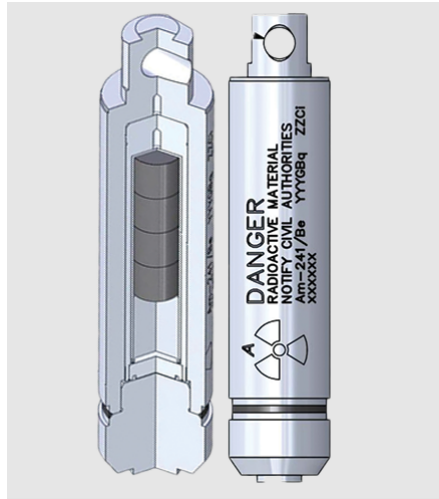
Fig. 1.5: The AmBe source for oil well logging. [19]

PuBe sources are not produced for approximately 40 years due to proliferation standards. Although there are still hundreds of such sources in Europe [20]. In contrast, AmBe sources can still be purchased, e.g., for well logging, radiography and tomography. Fig. 1.5 shows the AmBe capsule designed for oil well logging. The source is double-encapsulated in stainless steel.

1.1.3 Neutron sources based on gamma emitters

Unlike in the case of the previously described (α,n) sources, the spectrum of neutrons emitted by (γ,n) sources is almost monoenergetic. This is caused by the nature of γ spectra. As the converter material is used beryllium or deuterium, with (γ, n)

threshold of 1.665 MeV and 2.225 MeV, respectively. The production of neutrons is, in the case of a beryllium converter, described by the following equation:

$$^9\text{Be} + \gamma \to{}^8\text{Be} +{}^1\text{n}. \tag{1.2}$$

The γ source has to emit rays with energy above the previously mentioned thresholds and it has to have a relatively long half-life. According to these conditions, we can find only a few suitable sources - ^{124}Sb, ^{88}Y, and ^{226}Ra, where only with ^{226}Ra is possible to use both types of converters.

Tab. 1.2: The comparison of some radioisotopic sources by their half-life, neutron yield per Bq, and average neutron energy according to [21].

Source	Half-life (y)	Neutron yield (n/s·Bq)	Average E_n (MeV)
^{241}AmBe	432.6	$5.9 \cdot 10^{-5}$	4
^{241}AmB	432.6	$1.4 \cdot 10^{-5}$	3
^{239}PuBe	24110	$5.9 \cdot 10^{-5}$	4.5
^{252}Cf	2.647	0.12	2.3
^{88}YBe	0.29	$8.1 \cdot 10^{-5}$	0.2

The typical neutron energy is in the order of keV (see Tab. 1.2), compliant with applications that require thermal neutrons, such as Active NonDestructive Analysis (ANDA) [21]. SbBe is typically used as an external neutron source in power nuclear reactors. Fig. 1.6 shows an example of a secondary source assembly rod.
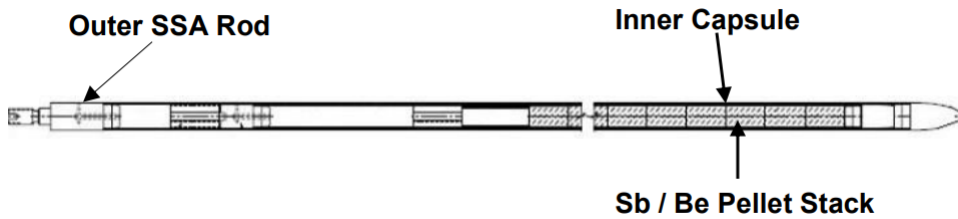
Fig. 1.6: The double encapsulated secondary source assembly by Westinghouse [22].

1.2 Neutron generators

Neutron generators are devices based on fusion reactions, the most common is the neutron production by reaction DD (Deuterium-Deuterium):

$$^2\text{H} +^2 \text{H} \rightarrow^3 \text{He} +^1 \text{n} \tag{1.3}$$

with neutron energy around 2.4 MeV or DT (Deuterium-Tritium):

$$^3\text{H} +^2 \text{H} \rightarrow^4 \text{He} +^1 \text{n,} \tag{1.4}$$

where the neutron energy is about 14.1 MeV. The neutron spectra for DD, DT, and TT (Tritium-Tritium) reactions are in Fig. 1.7, DT spectrum is also compared with the spectra of radioisotopic sources in Fig. 1.3 (iv).
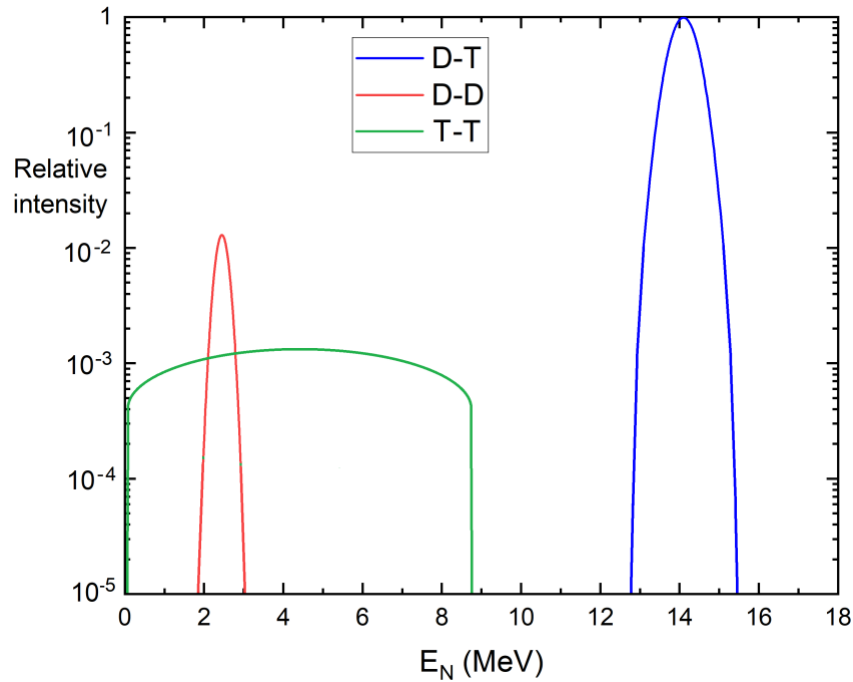
Fig. 1.7: The normalized neutron spectra for DD, DT, and TT reactions. [23]

Intensities are usually higher than 10^9 n/s. This kind of source is ideal for commercial usage, such as inspection of materials (e.g., aluminum or cement), land mine detection, cargo screening, etc. In addition, it is suitable for medical use in BNCT. Neutron generators, in contrast to the previous group of sources, can be operated either in pulse or continuous mode.

The following sections describe the available types of fusion-based sources.

1.2.1 Penning diode generators

The most common neutron generators in the world are based on Penning ion sources, the scheme is shown in Fig. 1.8. This kind of source consists of a hollow cylindrical anode with cathode plates at each end of the anode. The construction of the generator is the following: the electric field of the Pennning source ionizes the deuterium or tritium gas of pressure about 0.1 Pa and generates plasma. Ions coming from the plasma are accelerated by the diode structure forward to the metal hydride target. An external magnet is used for the generation of the coaxial magnetic field.

These sources are available in either DD or DT mode with neutron yields of $10^5 - 10^8$ neutrons/s and $10^7 - 10^{10}$ neutrons/s, respectively [6].
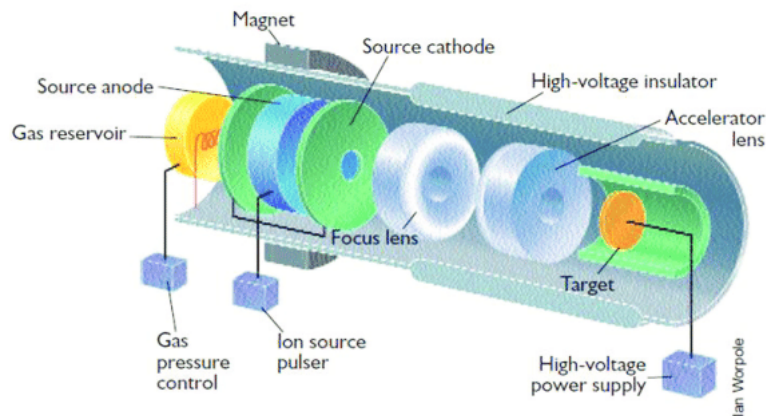
Fig. 1.8: The model of Penning diode-based neutron generator. [6]

1.2.2 Radio Frequency Induction (RFI) plasma generators

In this type of source, the ions come from the RFI plasma, and the same as in the previous case, after acceleration by the DC potential they hit the titanium target. These generators also called axial generators, because of the layout of all main components along one axis. The deuterium ions hit the target to form the titanium hydride in the thin surface layer. Consequently, other incoming deuterium ions interact with this titanium hydride which leads to the production of neutrons. To operate this source is necessary an active vacuum system. Usually, the neutron yield for the DD reaction reaches 10^8 neutrons/s, the new models (Fig. 1.9) can achieve 10^{10} neutrons/s [6].
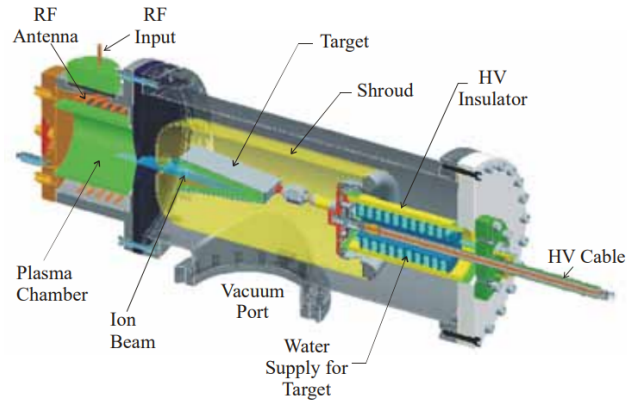
Fig. 1.9: The model of axial neutron generator. [6]

1.2.3 Inertial Electrostatic Confinement (IEC) plasma generators

The concept of IEC is based on confining plasma in a potential well of the electrostatic field, which can also be combined with the magnetic field. The field is created by grids or cathodes in spherical or cylindrical geometry. The example of such a device illustrates Fig. 1.10. Created ions are accelerated towards the center of the sphere/cylinder, passing through the transparent cathode, creating a virtual anode inside. This anode attracts cold electrons and thus it is created also virtual cathode inside the virtual anode [24]. Ions that escape from the potential well undergo mostly the Coulomb collisions, therefore, fusion yields for the IEC source are only about 0.01 % of the input power. However, in the case of some sources was achieved the neutron yield of 10^{10} neutrons/s [6].
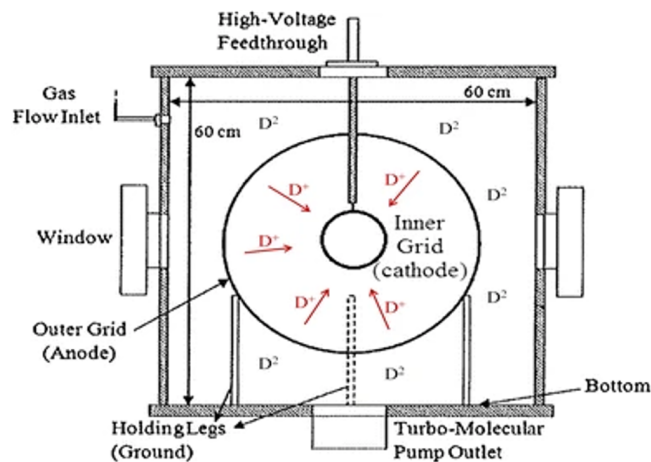
Fig. 1.10: The model of axial neutron generator. [24]

1.3 Accelerator-based systems

Interactions of accelerated charged particles with a relevant target can lead to neutron yields with a broad range of energies and various shapes of spectra. There are a lot of possible combinations of beam particles and target material, each with characteristic parameters. Additionally, the properties of individual components, such as the current of accelerated particles, their energy, or the thickness of the target, also influence the character of the produced neutron beam.

Charged particles [2], mostly protons, deuterons, or electrons, are injected into the particle accelerator to increase their energy. After this, the accelerated projectile hits the converter target. There are a lot of types of conventional particle accelerators in use with different parameters, i.e.:

- **Cockroft-Walton accelerator** applies the high voltage via the so-called voltage multiplier cascade or Cockroft-Walton generator with the aim of accelerating the particle. Nowadays their purpose is the primary acceleration of particles before their injection into a larger accelerating facility.

- **Van de Graaff accelerator** uses the same principle, but the source of high voltage is the Van de Graaff generator - the system of the metallic spherical electrode and conductive belt, attached to the electric motor. The belt carries the charge to the electrode, where the charge builds up. This type of accelerator was widely used during the 20th century; however, it is not so widespread nowadays.

- **Linear accelerator i.e. linac** (in Fig. 1.11) uses alternating voltage and a series of drift tubes. The particle is accelerated during the first half-wave of alternating current forward the following drift tube. This allows accelerating the particle forward, without the change in its direction during the second half-wave of the current. Their advantage is that it is possible to accelerate heavy ions, and the acceleration of electrons up to high energies is easier. On the contrary, to reach very high energy, it is necessary to build a long facility.

- **Cyclotron** is an accelerator, which requires also the presence of a magnetic field, perpendicular to the plane of motion of the accelerated particle. It benefits from the fact that for a constant magnetic field, the charge and mass of the particle, the increase in the radius of the path of the particle is connected with the increase of its velocity is taken into account also. This type

---

[2]Although the acceleration of a lighter particle is more convenient, the reaction probability does not change with the substitution of a projectile and target particle. There are efforts to develop a neutron source based on accelerations of lithium ions towards the proton target. This is advantageous because if a proton impinges the target nucleus, the produced neutrons are spread isotropically and it is required to accelerate protons to a higher energy than the heavier projectile, which leads to a forward-focused neutron beam [25].

of accelerator is widely used for its cost and size advantage in comparison to other accelerator types. On the other hand, the effects of relativity limit the maximal particle energy.

- **Betatron** accelerates electrons injected by the electron gun into the main ring (doughnut-shaped vacuum chamber), which is placed between the poles of the electromagnet driven by the alternated current.
- **Microtron** is a lot a like the cyclotron, but, meanwhile the cyclotron is based on classical mechanics, in the microtron the relativistic change of mass of the particle due to the increase of its velocity. Electrons are accelerated from the accelerator cavity and under the influence of the magnetic field, their path is circular, leading back to the cavity, where the electron gains additional energy. As the mass of the electron increases with its velocity, the diameter of its path also increases [26].
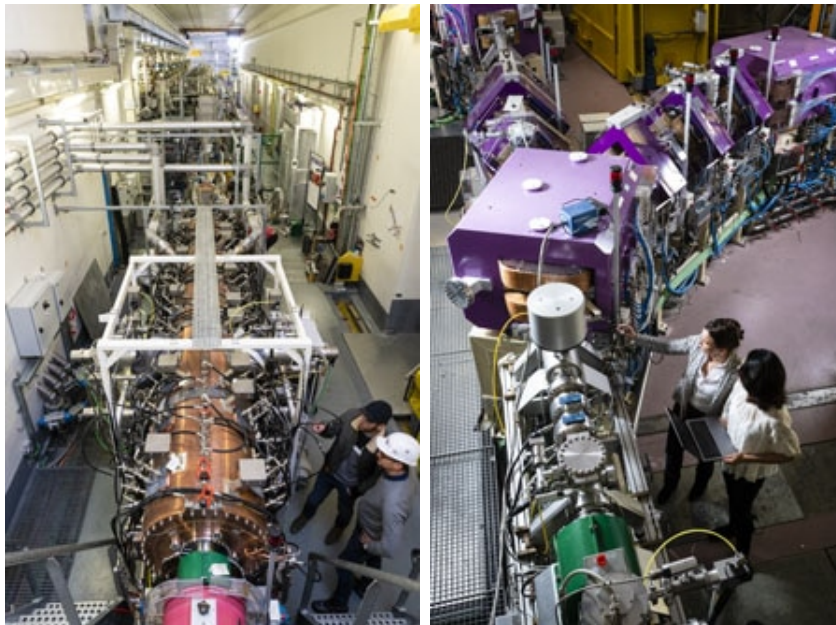
Fig. 1.11: An example of linac - the facility SPIRAL2 in Caen, France [27].

In addition to the above-mentioned devices, there are even more types or variations of those. It appears to be more advantageous to use deuterons as a projectile due to the additional neutron production via deuteron break-up[3]. In combination with the thick target, it is possible to gain an intense neutron flux with a continuous energy spectrum [28].

Moreover, it is possible to use a high-power laser instead of a conventional accelerator. The principle is the same, the accelerated particle interacts with the

---

[3]Deuteron break-up is the interaction of the deuteron with the target nucleus, which has the three-body result - the nucleus, proton, and neutron.

target nucleus, and this interaction leads to neutron production. The difference is that charged particles are created during the interaction of the laser beam with the proper target. The kind and energy of the produced particle depend on the parameters of the laser pulse and the material of the target [29].

1.3.1 Light targets

Usage of a light target allows accelerating projectile particles to the energy of units or tenths of MeV. It is possible to produce quasi-monoenergetic or white neutron spectra. The most common target materials are presented and current and future sources are listed in Tab. 1.3 and described below.

Deuterium can be used as a target not only in neutron generators but also in the case of the accelerator-based system. It benefits from the fact that the $D(d,n)^3He$ reaction leads to a high neutron yield in the forward direction. Additionally, the product of the reaction is not radioactive. It appears to be more convenient to use the heavy water jet target (in Fig. 1.12) than the deuterium jet target [30].
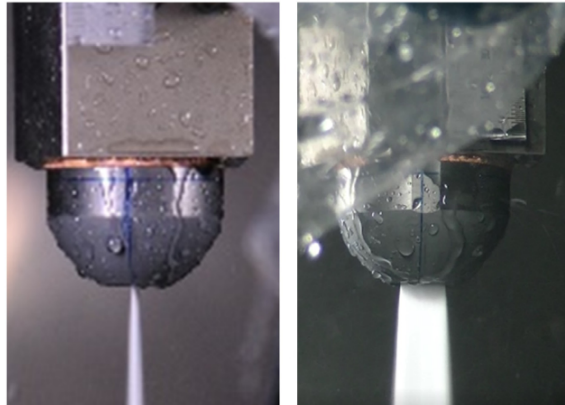
Fig. 1.12: The photo of a heavy water jet at speed approx. 220 m/s [30].

Lithium is a popular material because of the neutronics, especially in the case of $^7Li(p,n)^7Be$ reaction. This reaction has the threshold energy of 1.88 MeV. The usage of proton energy slightly above the threshold allows the gain of the neutron beam with energies in the order of tens of keV mostly in the forward direction. The downside of the usage of lithium is its large reactivity in combination with air, also its melting point is relatively low, compared to other possibilities (only 180.5 °C), and its thermal conductivity is not sufficient. For the reasons given above, the target is usually a thin layer applied on a supporting material (e.g. copper) with channels for water cooling [31]. The thin target leads to a quasi-monoenergetic neutron

spectrum, as was shown in Fig. 1.1.

Beryllium can be used both as a thin and thick target, depending on the required shape of the final spectrum. The usage of the thin target leads to quasi-monoenergetic spectra, but with higher production of lower energy neutrons than in the case of the thin lithium target. The usage of the target thick enough to stop all incident particles leads to a continuous spectrum (Fig. 1.13) [28].
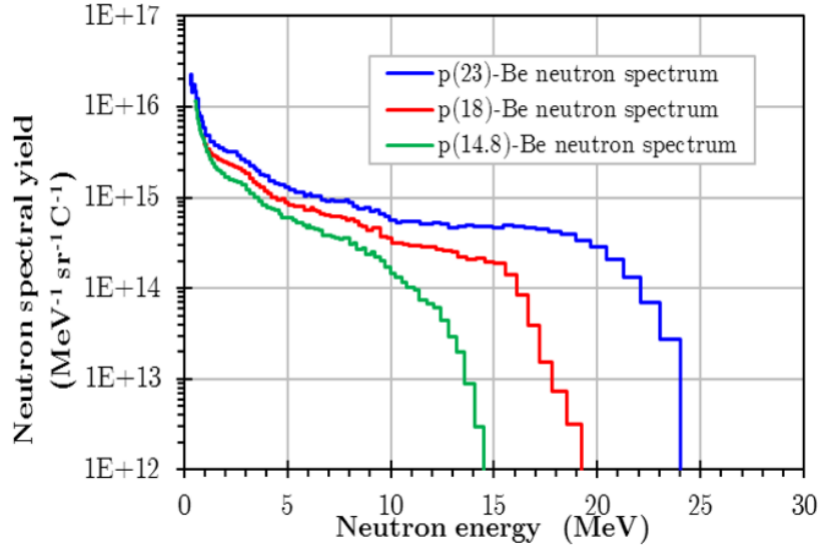
Fig. 1.13: The neutron spectra for p+Be using a thick target and three proton energies [32].

The main reason for the usage of beryllium is that its melting point is 1287 °C, which means much higher than in the case of lithium and therefore this target is more durable [32].

In addition to the materials mentioned above, other materials, for example, carbon [28] can be used. However, beryllium and lithium are selected in a larger number of cases.

These targets are usually considered for Compact Accelerator-driven Neutron Source (CANS). Due to the shutdown of a lot of research reactors in the near future, there will be a large drop in the neutron beam time. In Europe, it will depend mostly on a few facilities based on spallation reactions. It seems necessary to develop new facilities, which will be able to provide additional neutron beam time to ensure that it will be accessible to the scientific community. In addition, this is an opportunity to overlap the difference between low neutron fluxes from small neutron generators and large spallation-based facilities. Some of the CANS are summarized in Tab. 1.3 and described in the following paragraphs.

Tab. 1.3: The list of CANS. Facilities with dates marked with an asterisk (*) are in the beginning of 2022 under construction.

Source	Country	Projectile	Max. energy	Target	Commissioned
U-120-M	Czechia	p,d	55	Be	1977
iThemba LABS	South Africa	p	200	Li, Be	1980s
LENS	USA	p	13	Be	2009
KUANS	Japan	p	3.5	Be	NA
ESSB	Spain	p	50	Be	NA
PKUNIFTY	China	d	2	Be	2012
CPHS	China	p	13	Be	2013
RIKEN CANS	Japan	p	7	Be, Li	2013
TR-24	Czechia	p	24	Be	2015
Helsinki BNCT	Finland	p	2.6	Li	2018
NFS	France	p,d	40	Li, Be, C	2019
LINUS	Italy	p	5	Li, Be, W	2022*
SARAF	Israel	p,d	40	Li	2023*
DD at CAEP	China	d	11	D20	2025*
HBN	Germany	p	70	Ta	Concept
SONATE	France	p	3	Be, Li	Concept
NOVA ERA	Germany	p	10	V	Concept

Cyclotron U-120M and TR-24

The multipurpose particle accelerator U-120M at Řež, Czech Republic, was commissioned in 1977. It can accelerate protons up to 38 MeV and light ions. In combination with the beryllium target, it produces neutrons with energies 6-37 MeV by interactions of protons or deuterons. The other option is the flowing heavy water target, which leads to the production of neutron fluxes of up to 10^{11} neutrons/cm^{2}s at an energy extending 35 MeV.

Cyclotron TR-24 is operational since 2015 and it can provide protons with energy in the range of 18-24 MeV. The beryllium target to reach the neutron flux of 10^{12} neutron/cm^{2}s is under development [33].

Neutron source at iThemba LABS

The unique neutron source at iThemba Laboratory for Accelerator-Based Sciences (LABS), South Africa, offers neutrons with high energy, compared to other sources with the same target material. Protons are accelerated in the cyclotron up to the

energy in the range from 30 MeV to 200 MeV. After acceleration, they interact with a beryllium or lithium target, which is placed on the ladder, offering three positions for the target and one position for a quartz window [34].

Low Energy Neutron Source (LENS) Indiana

The CANS of the University of Indiana, USA, focuses, among others, on neutron moderator research. The LENS facility has been operational since 2009. It uses 13 MeV protons to gain neutrons from the beryllium target. It can use a relatively broad range of pulse width and repetition rate and it can be easily changed [35].

Kyoto University Accelerator-driven Neutron Source (KUANS)

At KUANS, the neutron source in Kyoto, Japan, the protons accelerated up to 3.5 MeV hit the beryllium target to produce neutrons. The target takes the form of a thin disc plate soldered to the niobium plate cooled by water. All residual protons that did not interact with beryllium are stopped in niobium [36].
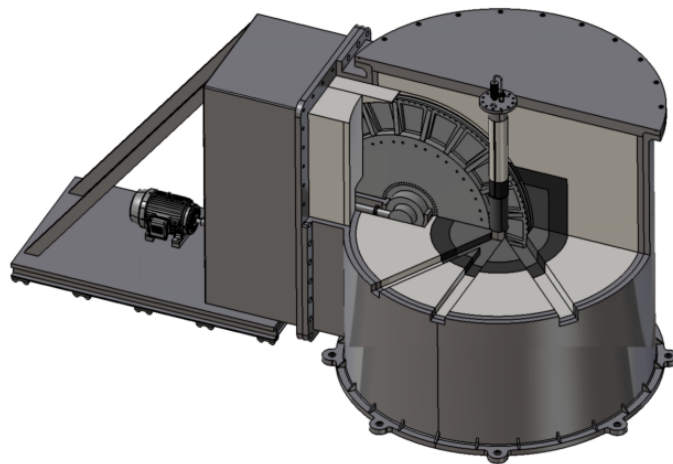
Fig. 1.14: The target vessel for the rotating target of ESSB [37].

European Spallation Source Bilbao (ESSB)

The ESSB aims to extend the European initiative of building the European Spallation Source by introducing a smaller neutron source in Bilbao, Spain. The facility consists of a linac, which accelerates protons up to the energy of 50 MeV with a peak current of 75 mA and a repetition rate in the range of 20 - 50 Hz. It is planned to upgrade the linac to get proton energy up to 200 MeV. The target is, as in the case of ESS at Lund, a set of plates attached to the rotating wheel. Fig. 1.14 shows

the model of the target vessel. In the case of ESSB, the material of the plates is beryllium as a compromise between the neutron yield and average neutron energy. The target station is cooled by water [37].

PeKing University Neutron Imaging FaciliTY (PKUNIFTY)

The CANS facility PKUNIFTY in Beijing, China, delivered the first neutrons in 2012. The PKUNIFTY is based on the coupling of the accelerator of deuterons with the beryllium target. The deuterons can reach the energy of 2 MeV, with a current of 4 mA, there can be a neutron flux of $3 \cdot 10^{12}$ neutrons/cm^{2}s, and the maximal current should be larger than 40 mA [38].

Compact Pulsed Hadron Source (CPHS)

Tsinghua University developed the CPHS, which was the first multipurpose pulsed neutron source in China. The facility has been operating since 2013. Protons can be accelerated up to 13 MeV and hit the beryllium target with moderators either solid methane or room-temperature water [39].

RIKEN Accelerator-driven Neutron Source (RANS) I and II

At RIKEN, Japan, another CANS is under development. The RANS-I run since 2013 and uses 7 MeV protons hitting a beryllium target to neutron yield 10^{12} neutrons/s. The RANS-II design aims to achieve the same current, i.e. 100 µA, but with proton energy of 2.5 MeV, which is suitable for the lithium target. Because the neutron energy is much lower for the lithium target than for the beryllium one (0.76 MeV and 5.1 MeV, respectively), the shielding can be modified [40].
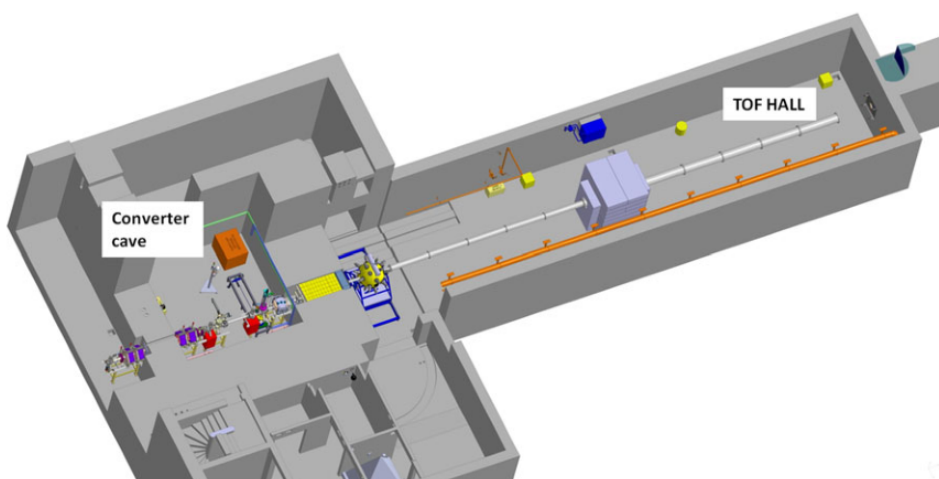
Fig. 1.15: The layout of the NFS area [28].

Helsinki BNCT facility

The first accelerator-based BNCT facility was installed at Helsinki University Hospital, Finland, in cooperation with Neutron Therapeutics Inc. It consists of an electrostatic proton accelerator, which delivers 30 mA of 2.6 MeV protons to the lithium target. The commissioning stage started in 2018 [41].

Neutrons For Science (NFS)

The NFS area (in Fig. 1.15) is part of the GANIL/SPIRAL-2 facility at Caen, France, and it is operational since 2019. The accelerator SPIRAL-2 is a linac with two ion sources (one for protons and deuterons, and the second one for heavy ions). It can deliver up to 5 mA beams of protons, deuterons, or heavy ions. The maximum energy differs in dependence on the type of an accelerated particle, from 14 MeV/A for heavy ions to 40 MeV for deuterons. It can operate with a thin lithium or beryllium target and produce quasi-monoenergetic neutron beams, or with a thick beryllium or carbon target to produce a continuous neutron energy spectrum [28].

Integrated LNL Neutron Source (LINUS)

The Laboratori Nazionali di Legnaro (LNL), Italy, created the project LINUS, based on existing accelerators. The proton linac, which delivers 5 MeV protons with an intensity of 40 mA, should be connected to beryllium and lithium targets. 70 MeV, 700 μA proton synchrotron will deliver protons to NEPIR (lithium, beryllium, or tungsten targets) and SLOWNE (tungsten target) facilities [42].

Soreq Applied Research Accelerator Facility (SARAF)

At Soreq Nuclear Research Center, Israel, was developed a unique liquid lithium target for a neutron source. The source is powered by an accelerator of both protons and deuterons with maximum energies of 4 and 5 MeV, respectively. The source can deliver neutrons up to energy of 20 MeV. It is scheduled to operate the facility with 40 MeV protons in 2023 [43].

DD source at China Academy of Engineering Physics (CAEP)

The CANS, which will be based on a heavy water target, is under development at CAEP, China, and its commissioning is planned for 2025. Deuterons, accelerated by linac up to energy 11 MeV at a frequency of 100 Hz with the average beam current of 0.33 mA, will interact with the heavy water jet target. The neutron energy should be in the range of 10-14 MeV. The angular neutron yield was calculated as $6.5 \cdot 10^{11}$ neutrons/s·sr [30].

High Brilliance Neutron source (HBN)

The aim of the project of the Jülich Centre for Neutron Science, Germany, is to develop a compact accelerator-based neutron source with high brilliance. The pulsed proton beam is supposed to reach the intensity of 100 mA at frequencies 24, 96, and 384 Hz and the proton energy of 70 MeV. Because of the relatively high projectile energy, the tantalum target was chosen. The density of power deposited in the target is 1 kW/cm^2, the microchannel cooling system should provide an adequate heat removal. The model of this target is in Fig. 1.16 Moderation down to thermal energy will be provided by polyethylene. Up to six neutron beam lines are planned to deliver neutrons to various instruments [44].
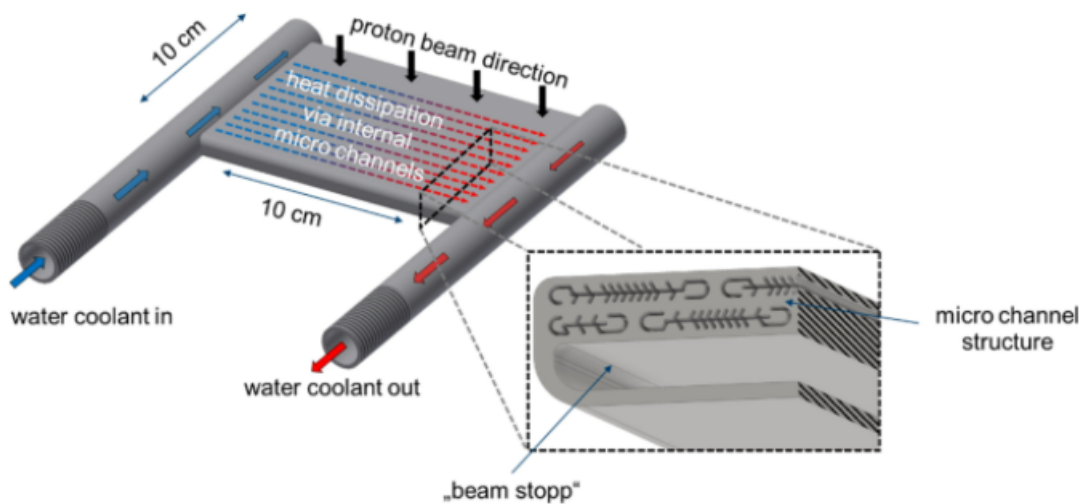
Fig. 1.16: The HBN tantalum target with microchannels [28].

SONATE CANS

The shutdown of the Orphée reactor at CEA-Saclay, France, was the impulse to the development of CANS, which would take advantage of the existing IPHI accelerator and deliver neutrons in the thermal energy region and sufficient flux. The protons can be accelerated in either pulsed or continuous mode up to the energy of 3 MeV, meanwhile the required intensity is between 20 and 100 mA. In the future, it is planned to increase the energy to 20 MeV. The prior is given to the consideration of the beryllium target, another possibility could be the liquid lithium target. The biggest challenge is to develop a target that will be able to withstand a power deposition of around 50 kW [45].

NOVA ERA

Another project of the Jülich Centre for Neutron Science, Germany. Calculations are based on the concept of protons accelerated up to 10 MeV with 1 mA intensity of the beam. Although most of the projects usually consider the beryllium target, because of the hazardous nature, the vanadium target was considered as an alternative, both in a circular shape with a diameter of 40 mm and thickness of 0.7 mm and 1 mm for beryllium and vanadium targets respectively. The water cooling is designed to dissipate the power of 400 W. For moderation to reach the thermal neutron energy region was offered polyethylene, the shielding is supposed to be assured by lead [46].

1.3.2 Spallation reactions in heavy nuclide target

Spallation reactions are exotic nuclear reactions, for which occurrence it is necessary to have the very high energy of an incident particle, typical for cosmic rays and the heavy nuclei target. The use of protons or deuterons with energy in the order of MeV or GeV is usually considered. To understand the process of the spallation reaction, which is also visualized in Fig. 1.17, it can be divided into several phases. The first
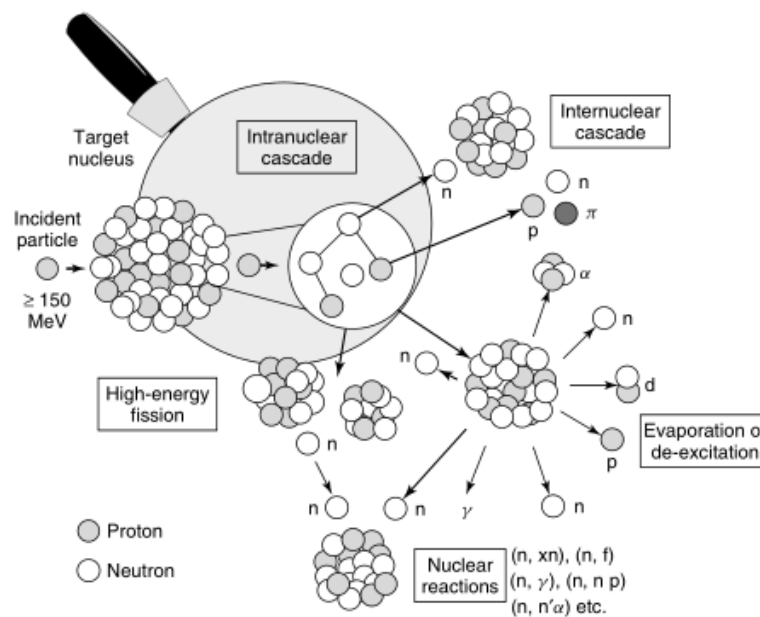
Fig. 1.17: The scheme of spallation reaction [9].

phase is called Intra-Nuclear Cascade (INC) and lasts for approx. 10^{22} s. The fast incident particle interacts with individual nucleons of the target nucleus, due to its small De Broglie wavelength in a series of elastic collisions. This leads to a cascade of collisions of target nucleons. Depending on the energy of the incident particle and

the number of nucleons in the target, there can also occur an emission of pions or even hadrons. If the particle has energy large enough to escape the original nucleus, it happens in the direction of the incident particle.

During the pre-compound phase, which occurs in less than 10^{18} s, it could be possible to observe pre-equilibrium emission - high-energy particles can be emitted after interactions in cascades.

The equilibrium phase is the last one. The energy is distributed among the nucleus which gets into the excited state. To get back to the ground state, the nucleus gets rid of excess energy by evaporation of neutrons or light fragments. If the excess energy is not large enough, it can also evaporate γ or β particles.

In the case of a thick target, the intra-nuclear cascade can occur. It is a result of the interaction of a high-energy emitted particle with the other target nucleus.

The advantage of the use of spallation reactions is that every reaction leads to the production of tens of neutrons, dependent on the incident particle energy and the type of target nucleus [9]. Table 1.4 contains a list of sources of spallation neutrons around the world.

Tab. 1.4: List of spallation neutron sources. protons are projectile particles at all of the mentioned facilities. Facilities with dates marked with an asterisk (*) are in the beginning of 2022 under construction.

Source	Country	Energy (GeV)	Target	Commissioned
SNS in LANSCE	USA	0.8	Pb	1972
ISIS	UK	0.8	W, Ta	1984
SINQ	Switzerland	0.57	Pb	1996
n_TOF	Switzerland	20	Pb	2002
SNS	USA	1	Hg, (W)	2007
J-PARC SNS	Japan	3	Hg	2008
CSNS	China	1.6	W	2018
ESS	Sweden	2	W	2025*

Los Alamos Neutron Science Center (LANSCE) neutron sources

There are several neutron sources at LANSCE, USA. The one described here is operational since 1972. Currently, it is being upgraded, so the linear accelerator will be able to provide 800 MeV protons with a continuous current of 1.25 mA. The standard is to use the annular lead target. Various neutron flight paths take advantage of changes in the angular distribution of neutrons produced at the spallation target.
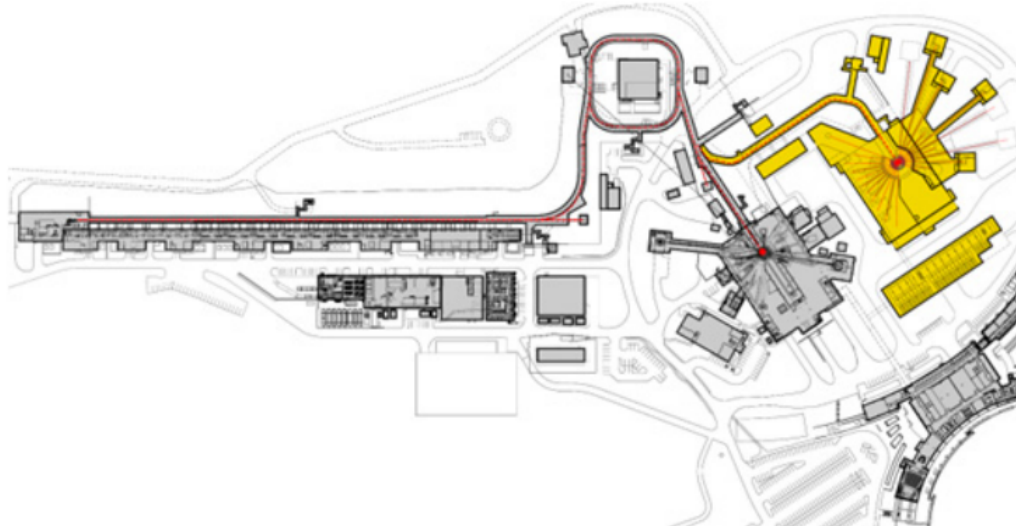
Fig. 1.18: The layout of SNS (the yellow part is the second target system) [51].

A Fusion Prototypic Neutron Source (FPNS) target is under development. It will benefit from the placement of fusion material inside the annulus [47].

ISIS Neutron and Muon Source

At ISIS, UK, the protons can be accelerated up to energy 800 MeV. There are two lines of proton beams that lead the beam to the appropriate target for neutron or muon production. There are two target stations for neutron production - TS-1 is a rectangular block of twelve plates, TS-2 is a cylinder. Both target stations are made of tungsten with tantalum cladding, and both are cooled by water [48].

Swiss Spallation Neutron Source (SINQ)

The spallation neutron source at Paul Scherrer Institute (PSI), Switzerland, is powered by the accelerator, which delivers protons with energy up to 570 MeV at the current of 1.8 mA. The target consists of a series of lead rods enclosed in zircaloy tubes and it is cooled by heavy water. The final neutron flux is in the order of 10^{14} neutrons/cm^{2}s. The SINQ is operational since 1996, in 2019-2020 all original neutron guides were exchanged. Now there are seven neutron guides, eight will be added in 2022 [49].

Neutron Time-of-Flight facility (n_TOF)

The n_TOF facility is in operation at CERN, Switzerland, since 2002. It uses 20 GeV protons accelerated by Proton Synchrotron in a pulsed regime with 6 ns

pulses. The target is made of lead and cooled by water. The neutron spectrum is wide, from 1 eV up to 250 MeV [50].

Spallation Neutron Source (SNS)

The Oak Ridge National Laboratory (ORNL), USA, operates SNS (in Fig. 1.18), which was commissioned in 2007. The original target system is liquid mercury sealed in the steel structure, with a moderator above and under the target. The second target system, currently under development, will be composed of rotating tungsten with a beryllium reflector. The proton energy is 1 GeV, the ongoing project Proton Power Upgrade will result in an increase in the proton beam power from 1.4 to 2.8 MW [51].

Japan Proton Accelerator Research Complex (J-PARC) SNS

The spallation neutron source at J-PARC is operational since 2008. It uses an accelerator with a repetition rate of 25 Hz to hit the target with 3 GeV protons, the maximal delivered power was 1 MW. The target material is mercury, which life-time was improved by the injection of microbubbles. The cavitation damage caused by the large power of incident particles is the reason to improve the target design and the way in which it couples with the water cooling system [52].

China Spallation Neutron Source (CSNS)

Dongguan, China, is the site of CSNS, which construction was completed in 2018. It is based on a linear proton accelerator and proton synchrotron. The project aims to achieve proton energy of 1.6 GeV at a repetition rate of 25 Hz, while delivering the power of 100 kW (or 400 kW in the future). The target is composed of 11 tungsten slices with tantalum cladding, cooled by water [53].

European Spallation Source (ESS)

The facility located in Lund, Sweden, is designed to produce neutrons by spallation reaction of protons with maximal kinetic energy of 2.0 GeV and the tungsten target. It is supposed to be operational at full performance in 2025. In that time ESS will deliver protons by linac with an average power of 5 MW, a pulse repetition rate of 14 Hz, and with the energy of one pulse of 357 kJ. The target consists of tungsten blades mounted on a wheel (see Fig. 1.19) which rotates 23.3 times per minute, cooled by helium. Neutrons are slowed down and guided to individual instruments [54]. Whereas the ESS aims to be a pan-European facility, the BrightnESS program [55] was established to enable international cooperation.
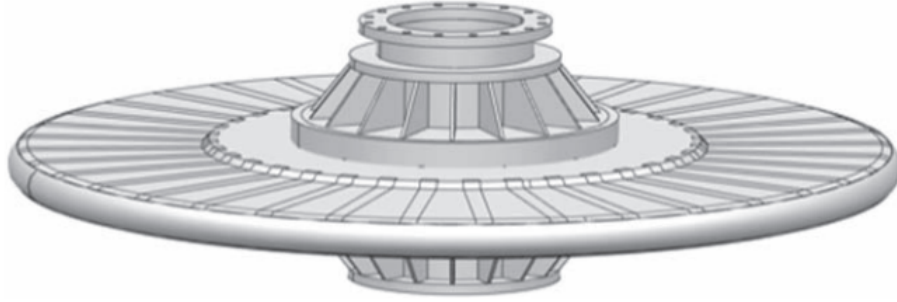
Fig. 1.19: The target wheel of ESS [54].

1.3.3 Photonuclear reactions in heavy nuclide target

The interaction of electrons with the heavy target nuclei results in Bremsstrahlung, high-energy photon production. Consequently, these high-energy photons interact with the surrounding matter via reactions such as (γ,n), $(\gamma, 2n)$, (γ,f). This matter can be the same as the source of photons, or it can be a secondary target (such as beryllium). Table 1.5 summarizes the operational facilities based on this type of neutron production.

Tab. 1.5: The list of photonuclear neutron sources. Electrons are projectile particles at all of the mentioned facilities.

Source	Country	Energy (MeV)	Target	Commissioned
GELINA	Belgium	140	U	NA
CANS at CAB	Argentina	25	Pb	1969
HUNS	Japan	34	W, Pb	1973
MT25	Czechia	25	Pb, U	1981
IREN	Russia	212	U, W	2009
nELBE	Germany	40	Pb	2013
Mobile NS	Japan	3.95	W, Cu, Be	NA

Geel Electron LINear Accelerator (GELINA) Neutron Source

The GELINA neutron source is operated at Geel, Belgium. The linear accelerator delivers electrons of energy 70-140 MeV with the maximal repetition rate of 800 Hz and 1 ns pulses. The target consists of depleted uranium and it is cooled by mercury, the produced neutrons can reach the maximum energy of 20 MeV. The facility offers 12 neutron beam lines and several measurement cabins [56].

CANS at Centro Atómico Bariloche

The compact system developed at Bariloche, Argentina, is based, unlike most of the presented CANS, on the electron linac, operating since 1969, which accelerates electrons up to 25 MeV with typical repetition rates of 12.5, 25, 50, and 100 Hz. The lead target is cooled by water and the type of a moderator depends on the requirements of the specific conducted experiment [57].

Hokkaido University Neutron Source (HUNS) I and II

The neutron source at Hokkaido, Japan, serves for the production of neutrons and x-rays. Its construction was completed in 1973. Accelerated electrons reach the energy of 34 MeV, current of 35 µA, and repetition rate of 50 Hz. The target consists of a tungsten plate and blocks of lead cooled by water. The upgrade of the target and moderator system is ongoing to improve the neutron yield [58].

Microtron MT25

The Microtron MT25 electron accelerator in Prague, Czech Republic, is operational since 1981. The facility offers the possibility of producing neutrons through the interaction of electrons of maximal energy of 25 MeV, repetition rate of 423 Hz, and pulse length of 3.5 µs, with a lead or uranium target. The neutron energy can reach (in the case of the lead target) 2 MeV [33].

Intense REsonance Neutron source (IREN)

The IREN facility (in Fig. 1.20) was developed at JINR, Russia, and its operation began in 2009. The electron linear accelerator LUE-200 is projected for the peak current of 1.5 A with the repetition rate 150 Hz, and neutron energy of 212 MeV. Electrons can irradiate the uranium or tungsten target, the neutron intensity should reach $2 \cdot 10^{13}$ neutrons/s [59].

neutron source at Electron Linear accelerator with high Brilliance and low Emittance (nELBE)

The neutron source at Forschungszentrum Dresden-Rossendorf, Germany, started its operation in 2013 and it is based on the Electron Linear accelerator with high Brilliance and low Emittance (ELBE) facility. The maximal electron intensity is 1 mA with the energy of 40 MeV, and repetition rate of 26 MHz, with pulse width smaller than 10 ps. The target consists of a loop of liquid lead, driven by an electromagnetic pump. There is produced bremsstrahlung, which irradiates the molybdenum tube to produce neutrons [60].
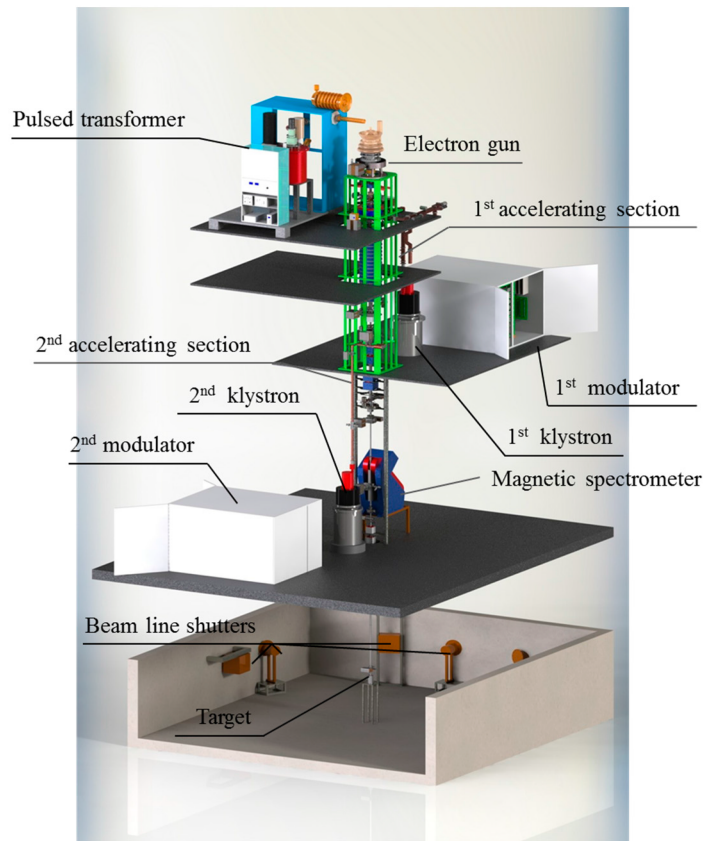
Fig. 1.20: The layout of IREN facility [59].

Mobile X-band neutron source

The portable neutron source based on electron linac was developed at the University of Tokyo, Japan. The linac delivers 3.95 MeV electrons to the tungsten/copper target for photon production. The beryllium target was adopted for neutron generation because of the low threshold energy of the reaction [61].

1.4 Reactors

According to the IAEA Research Reactor Database, since the 1950s, 842 research reactors have been built to this day. Currently, there are 220 operational research reactors in the world (52 of them are in Russia and 50 in the USA, the distribution is in Fig. 1.21). The other 24 of them are either under construction or planned [62]. Due to the aging of these reactors, many of them will be shut down in the following years. The purpose of these reactors varies. Some focus on the measurement of nuclear data, some on isotope production, training and education, testing of individual components, etc.
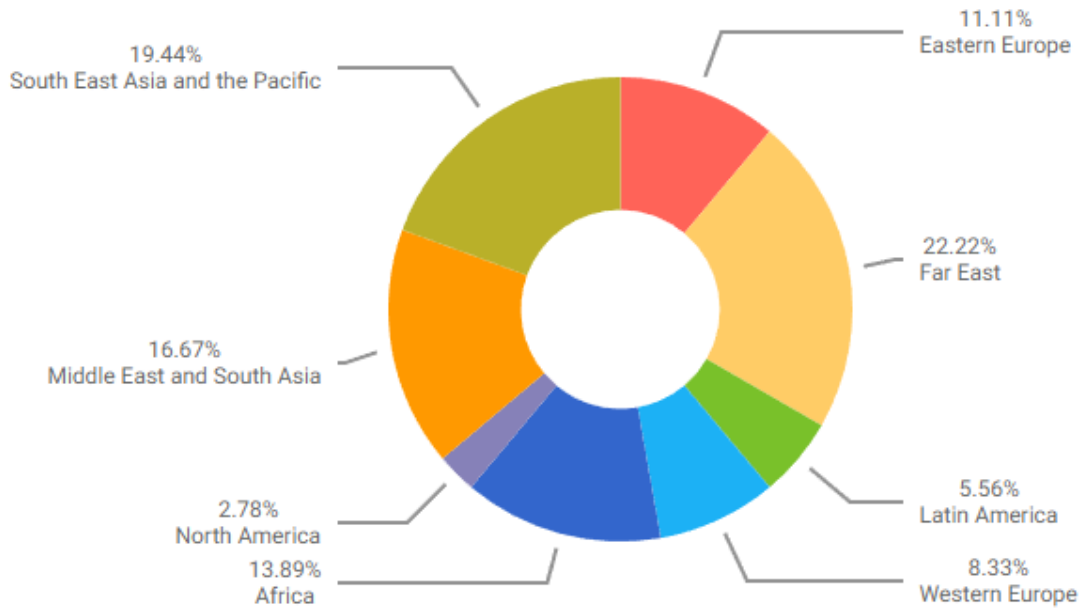
Fig. 1.21: The regional distribution of operational research reactors [62].

Usually, Low Enriched Uranium (LEU) is used as fuel, and its most common shape is a plate. Neutrons produced by fission are fast, with the energy around 2 MeV. Whereas it is required to deliver neutrons mainly in the thermal or cold energy range, it is also important to select an appropriate moderator.

The reactors described in the following paragraphs present only a small sample of all research reactors. Selection is focused primarily on large research structures and on projects that are under construction or planned. Tab. 1.6 summarises the reactors described in this thesis.

LVR-15 Research Reactor

The research reactor LVR-15 at Řež, Czech republic, is a light water pool type reactor with maximum power of 10 MW. The fuel is 19.75 % enriched uranium IRT-4M type. Water combined with beryllium serves as a reflector. The reactor reaches the maximum thermal flux 10^{18} neutron/m²s. The reactor went critical at first in 1957 [33].

Budapest Research Reactor (BRR)

The BRR, which layout is in Fig. 1.22, is a VVR-type research reactor, functional since 1959 in Budapest, Hungary. Its thermal power is 10 MW and the maximal thermal flux is $2.1 \cdot 10^{14}$ n/cm²s. Since 2012 is the reactor operated with 20% enriched

Tab. 1.6: List of research reactors that were selected to be described in this work. Facilities with dates marked with an asterisk (*) are in the beginning of 2022 under construction.

Reactor	Country	Type	Commissioned
LVR-15	Czechia	Pool	1957
BRR	Hungary	VVR	1959
JRR-3M	Japan	Pool	1962
HFIR	USA	Tank	1966
ILL HFR	France	Heavy water	1971
MARIA	Poland	Pool	1974
IBR-2	Russia	Pulsed	1978
FRM II	Germany	Pool	2005
OPAL	Australia	Pool	2007
PIK	Russia	Tank	2022*
RA-10	Argentina	Pool	2022*

VVR-M2 type fuel. Various neutron guides, 10 horizontal and 45 vertical channels offer a lot of possibilities in various science branches, mainly with thermal and cold neutrons [63].

JRR-3M at Japan Atomic Energy Agency (JAEA)

The reactor at JAEA, Japan, is operational since 1962. It was modified in the 1990s to reach the thermal power of 20 MW. It is a pool-type reactor, moderated and cooled by water. The maximum thermal neutron flux is $3 \cdot 10^{18}$ neutrons/m²s. The reactor was shut down from 2010 until 2021, the periodical shut down was extended due to the earthquake in 2011 [64].

High Flux Isotope Reactor (HFIR)

The HFIR facility is operated by ORNL, USA, since 1966. Its thermal power is 85 MW and it is a pressurized, tank type, water-cooled, and water-moderated reactor. It undergoes modernization to deliver neutrons for a longer period. A part of this modernization is the transition from HEU to LEU (19.75%) [65].

High Flux Reactor (HFR) at Institute Laue-Langevin (ILL)

The ILL, that operates HFR is situated in Grenoble, France. It started its operation in 1971; later, in the 1990s, the entire reactor vessel was replaced, and a new
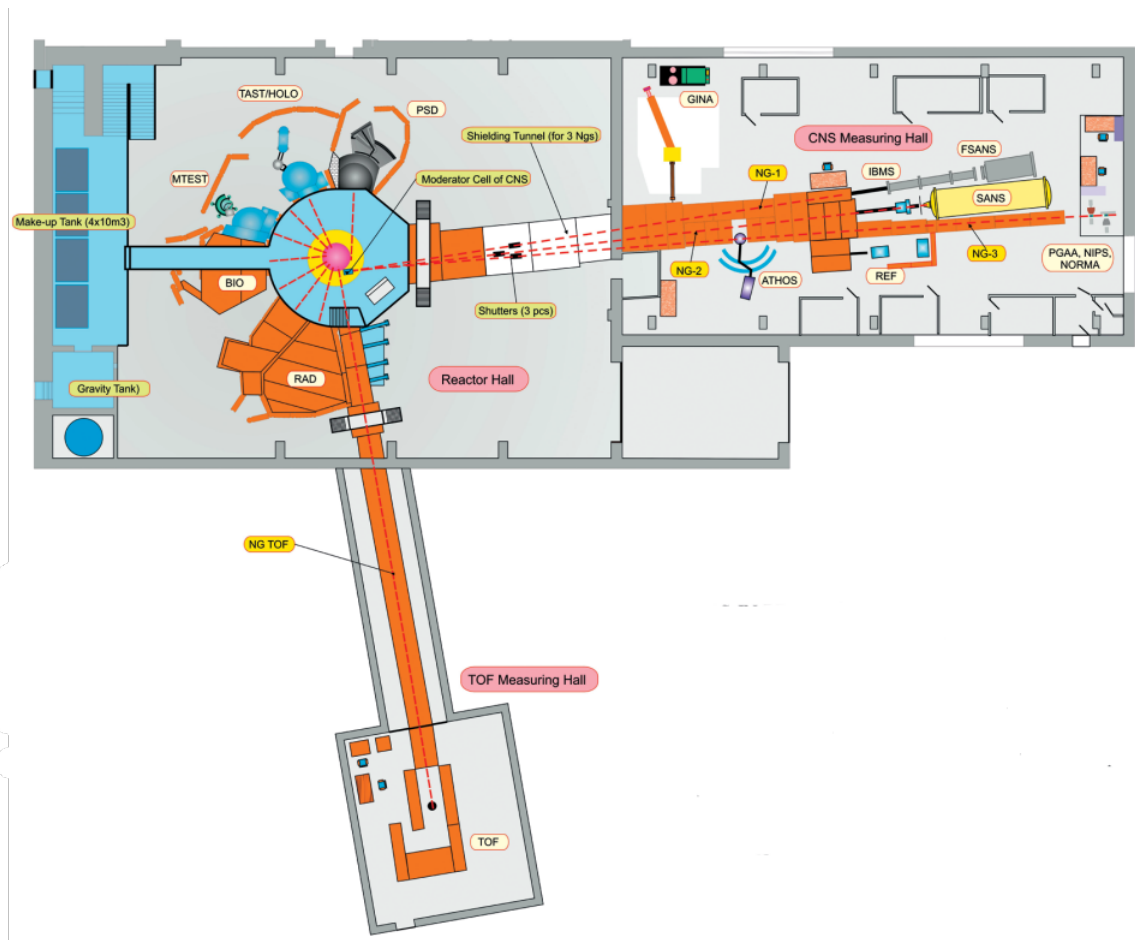
Fig. 1.22: The layout of the BRR facility [63].

operation started in 1995. The HFR is moderated and cooled by heavy water, it consists of only a single fuel element, 10 kg of highly enriched uranium. Its thermal power is 58.3 MW and produces the neutron flux of $1.5 \cdot 10^{15}$ neutrons/cm²s which is the highest in the world nowadays. There are around 40 instruments for individual experiments [66].

MARIA Research Reactor

The only nuclear reactor in Poland, the MARIA reactor, is situated at the Institute of Nuclear Research in Świerk. The reactor started its operation in 1974 and its purpose is mainly isotope production. It is a pool-type reactor of thermal power of 30 MW with U_3Si_2 fuel, graphite reflector, and water and beryllium moderator. The thermal neutron flux can reach $5 \cdot 10^9$ neutrons/cm²s [67].
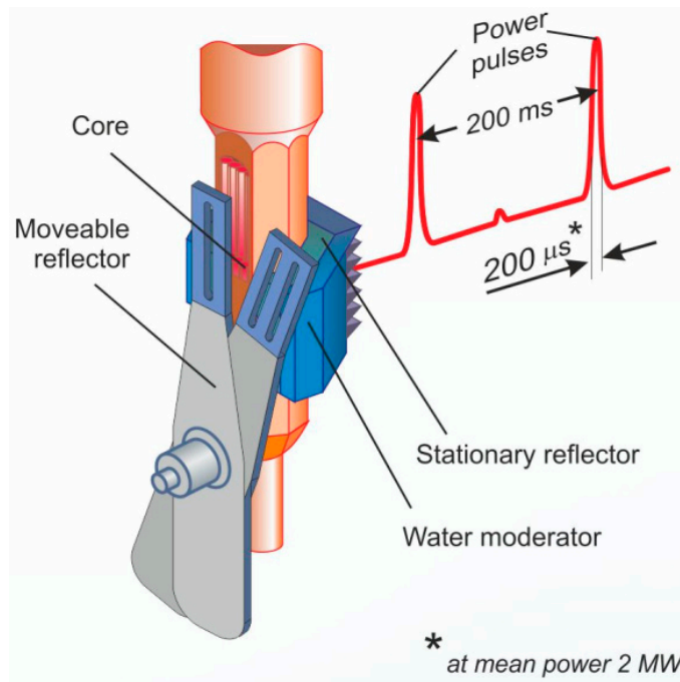
Fig. 1.23: A visualisation of the IBR-2 reactor [59].

IBR-2 reactor

The IBR-2 reactor (in Fig. 1.23) is a high-flux pulsed reactor operational since 1978 at JINR, Russia. Its thermal power is 2 MW. The fuel consists of pellets of plutonium dioxide. The pulse character of the reactor is given by the movement of two - main and auxiliary - movable reflectors. When both reflectors meet in front of the core, the reactor goes supercritical. The pelletized moderator is based on aromatic hydrocarbons and the average thermal neutron flux in the pulse is of the order of 10^{13} neutron/cm^{2}s [59].

Forschungsreaktor Munchen (FRM-II)

The German research reactor FRM-II is a pool-type reactor with thermal power of 20 MW and a maximum neutron flux of $8 \cdot 10^{14}$ neutrons/cm^{2}s. The view of the reactor is in Fig. 1.24. The fuel is manufactured by FRAMATOM and consists of U_3Si_2 in form of plates and the enrichment of uranium is higher than 90 %. The reactor is functional since 2005 and some instruments are still under development. There are 10 beam tubes that provide neutrons with a broad range of energies for single experiments and one tube, which provides positrons via interaction of neutrons with cadmium [68]. The reactor was temporarily shut down at the beginning of the COVID pandemic in 2020 and it should start up again in 2022 [69].
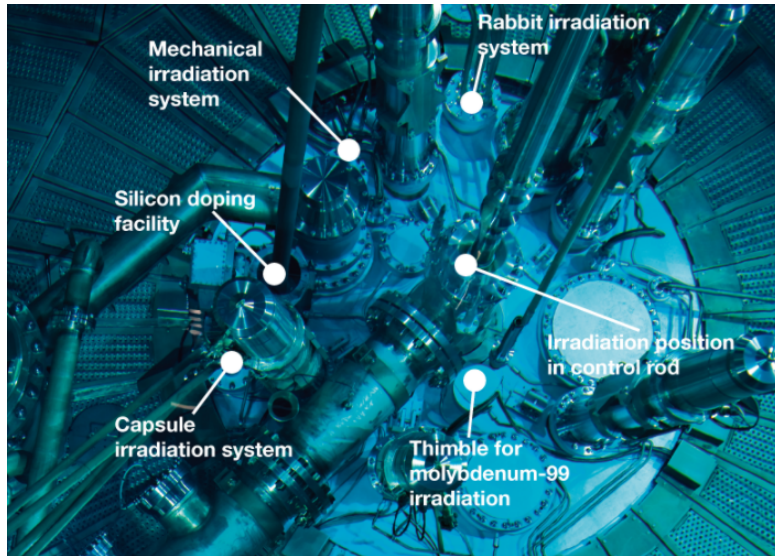
Fig. 1.24: The FRM-II reactor pool and irradiation facilities [68].

Open Pool Australian Lightwater reactor (OPAL)

The OPAL multipurpose research reactor is situated at the Australian Nuclear Science and Technology Organisation (ANSTO), Australia, and it is operated since 2007. The pool-type reactor uses LEU fuel in 16 fuel assemblies, cooling is provided by water, and zirconium alloy serves as a reflector [70].

Russian high-flux reactor PIK

The PIK reactor of Kurchatov Institute in Gatchina, Russia, reached criticality in 2011, nowadays it operates with the thermal power of 100 mW and the reach of full power, i.e., 100 MW should be between 2022 and 2024. The fuel is 90 % enriched uranium in the copper-beryllium matrix, the coolant is light water, and the moderator is heavy water. The maximal thermal neutron flux is $5 \cdot 10^{15}$ neutrons/cm^{2}s [71].

RA-10 Argentina Research Reactor

The open pool reactor of thermal power 30 MW is under construction at Ezeiza Atomic Centre, Argentina. The flux $3 \cdot 10^{14}$ neutrons/m^{2}s is expected. The fuel will be low enriched uranium silicide plates. The commissioning of the reactor is planned to the 2022 [72].

2 Cross-Sections

A wide spectrum of techniques of neutron production and the possibilities of their use were described. The main characteristic is that they are based on the interactions of ionizing particles with other materials. It is essential to understand how various materials interact with ionizing particles. The so-called term "cross-section" is used to describe these interactions. The term is often explained as the probability of the currency of a certain interaction. We distinguish between microscopic cross-section σ and macroscopic cross-section Σ.

If incident particles collide with the target nuclei, the microscopic cross-section is the ratio of the reaction rate of the observed reaction to the flux. The other explanation of this term is, that microscopic cross-section is the effective area of the target nucleus, through which the incident particle has to pass to cause certain reactions. According to this definition, it is noticeable, that the unit of the microscopic cross-section is cm^2. Since 1 cm is too large for the description of lengths within the meaning of the size of the nucleus, it is usually used the unit barn (1 barn = 10^{-24} cm^2). The product of the microscopic cross-section and material number density is the macroscopic cross-section with the unit 1/cm [73]. In this thesis will be the term cross-section used for microscopic cross-section.

Researchers from laboratories worldwide contribute to libraries of evaluated cross-section data, such as ENDF (USA), JEFF (EU), etc. Experimental results of cross-section measurements are stored in the international database EXFOR. To maintain the consistency, the data are stored in the ENDF-6 format.

The demand for experimental data is large because they are needed for the verification of physical models, which describe the behavior of particles. The EXFOR database contains more than 19 million data points. The highest number of data is available for uranium (12.1 %), carbon (9.22 %) and hydrogen (7.41 %) [78]. However, the lack of experimental data in the case of other elements and in the case of high energies of incident particles is significant.

2.1 Neutron interactions

The term cross-section describes the interaction of the incident particle with the target nucleus. Its value depends on the target, the type of an incident particle, its energy, and the type of interaction. The total cross-section is used to describe the probability that any of the possible particle interactions can occur.

The neutron interactions can be divided into two main branches - scattering and absorption. By scattering, we understand that the collision of the neutron with the target nucleus can lead to a change in the direction and velocity of the neutron, but
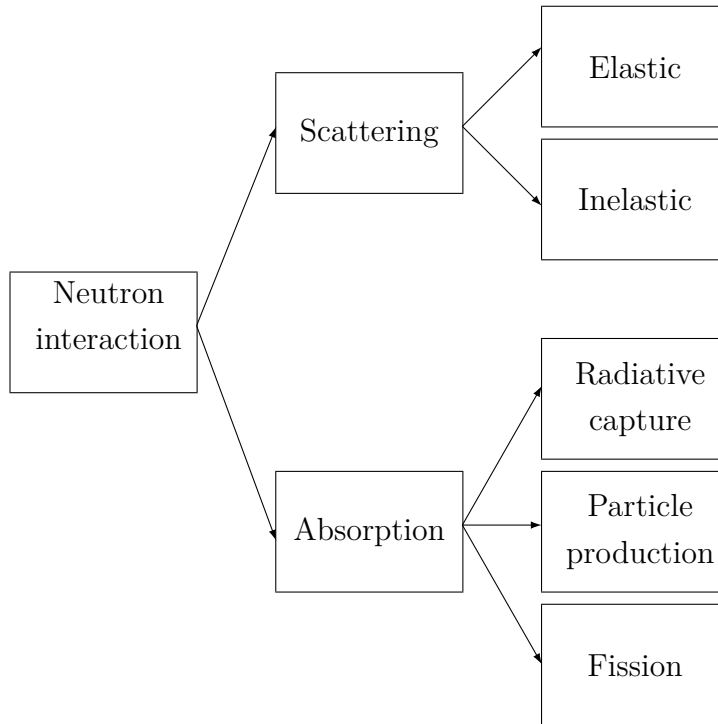
Fig. 2.1: The scheme of essential neutron interactions.

the target nucleus stays in the same composition, i.e., the number of either protons and neutrons remain the same. If the total kinetic energy of the entire system is conserved, the interaction is called the elastic scattering. If the nucleus is left in an excited state and part of the original neutron kinetic energy is used to get the nucleus to that state, wit is used the term inelastic scattering.

The absorption of the incident neutron by the target nucleus can lead to various products. The radiative capture leads to the release of excess energy in the form of γ rays. The other possible product is the charged particle, such as a proton, deuteron, or an α particle. Another outcome of this interaction can also be the production of more neutrons, the combination of particles, or fission [75]. The simple scheme of neutron interactions is in Fig. 2.1. In general, to measure neutron cross-sections, it is necessary to choose the most suitable neutron source, according to the interaction of the interest. The parameters of the source have to be selected to maximize the number of investigated reactions.
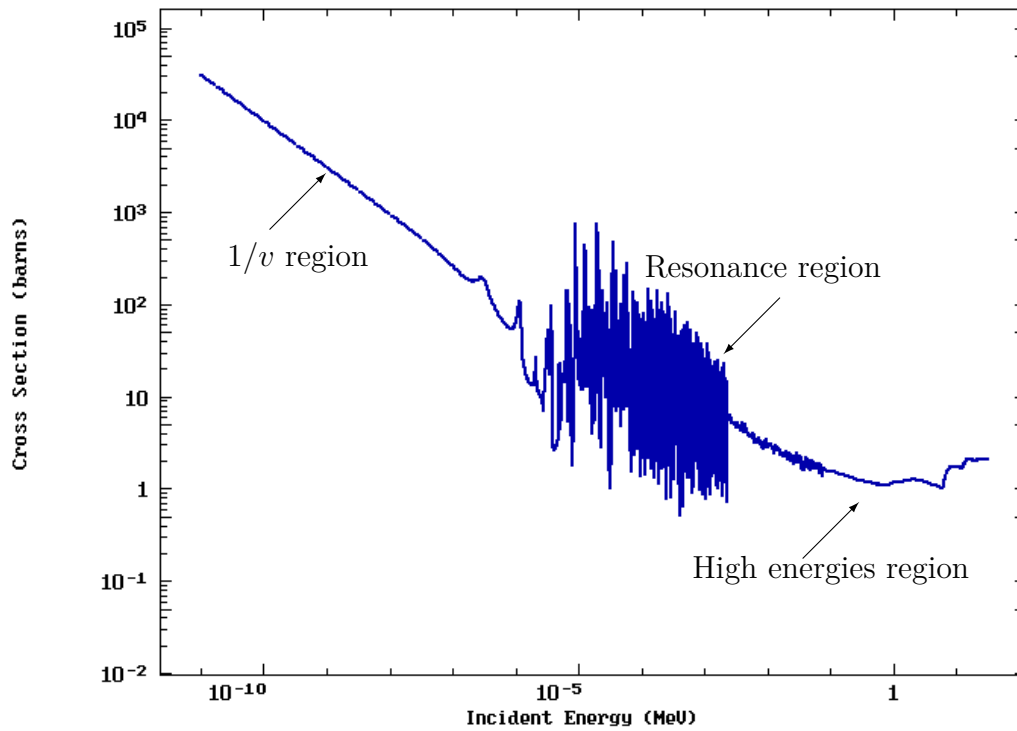
Fig. 2.2: Fission cross-section of ^{235}U [76] with the description of individual regions.

2.1.1 Energy regions

The cross-sections of neutron interactions show different behavior depending on the neutron energy. According to this, it is possible to observe three main energy regions:

- $1/v$ region, where the σ is inversely proportional to the velocity of the neutrons (energies lower than 1 eV),
- resonance region, where the dependence is generally $1/v$, but if the neutron energy corresponds to excited states of the produced nuclei, the result is the increase of the σ in order of a few magnitudes (energies from 1 eV to tens of keV) and
- high energies region, where the single resonances merge and thus the excitation curve is smooth. It is possible to observe threshold reactions.

Individual regions are marked in Fig. 2.2.

2.1.2 White spectrum

Sources of white spectrum neutrons are advantageous for measurements of cross-sections in $1/v$ and resonance regions. The neutron energy is measured via Time-of-Flight (TOF) [1] method and the products of the reaction are measured online, via observation of prompt γ-rays or recoiled particles. The TOF requires large distances between the neutron source and the measured sample, because the longer the path of the neutron, the higher the precision of the estimation of its energy. Halls for these measurements can be tens of meters long. Such configuration results in a lower neutron flux at the sample position. For measurements in the high energy region is necessary high neutron flux (σ are lower). According to this, it appears more suitable to use a quasi-monoenergetic neutron source.

2.1.3 Quasi-monoenergetic spectrum

As was mentioned, this type of neutron spectrum is usually used to measure cross-sections at high energies regions, mainly threshold reactions such as (n, xn). The sample is irradiated close to the neutron source, where the neutron flux is high. The radioactive products are measured offline via γ-spectrometry, for stable isotopes can be used mass spectroscopy. The main object of this thesis is to estimate cross-sections of reactions of neutrons from a quasi-monoenergetic source. Thus, the next chapter describes the methodology of such a process.

---

[1]The TOF is based on the evaluation of the neutron velocity from the known neutron path and measured time, which took neutrons to overcome the distance. This time is estimated from the primary signal (such as γ-ray) and the final signal when neutron impinges the detector matter.

3 Methodology

The measurement of neutron cross section via the γ-spectrometry is based on the fact, that the observed neutron interaction leaves the nucleus in an excited state. The nucleus emits a γ photons to deexcite itself. The energy of the photon corresponds to the difference between the original and final state. This difference is individual for every nucleus, thus, it is possible to identify the radionuclide based on its γ lines.

To obtain the final cross-section of observed interaction are necessary steps which will be described in the following chapters.

3.1 Gamma spectra

Measurement of γ spectra can be done with the HPGe (High Purity Germanium) detector. The principle of neutron detection is that the conductivity of a germanium semiconductor is proportional to incoming γ particles. Thus, the interaction of a photon with germanium leads to an electric pulse. Three main ways in which can γ particle interact with the matter of the detector, and which leads to the release
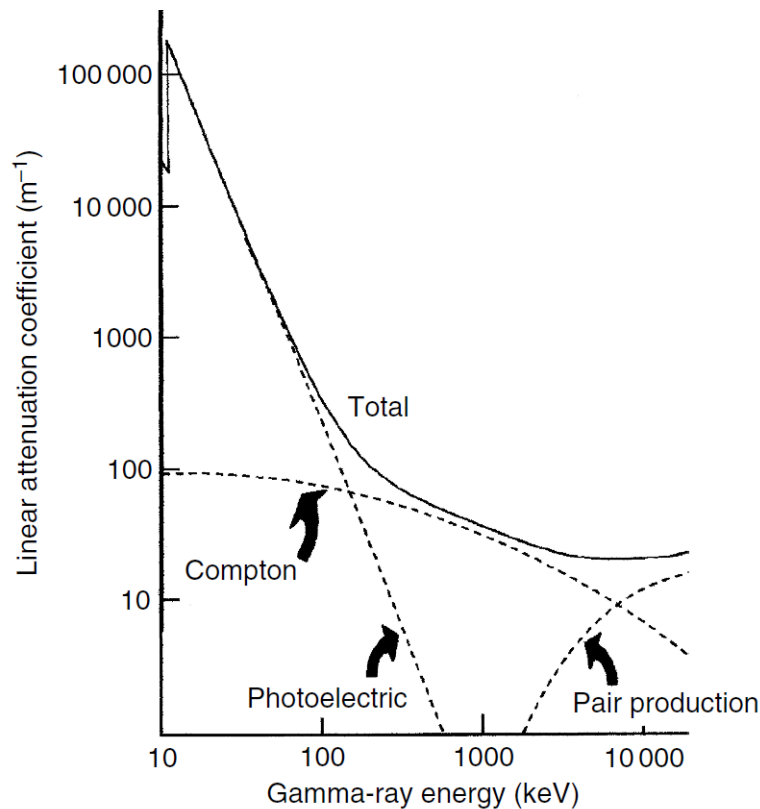
Fig. 3.1: The linear attenuation coefficient of germanium and individual contributions [77].

or creation of electron, are the photoelectric effect, the Compton scattering, and the production of pairs electron-positron. The contribution of individual effects to the attenuation of the γ photon in germanium is visualized in Fig. 3.1. This curve characterizes the response of the HPGe detector to γ rays.

3.1.1 Photoelectric effect

To understand this interaction, it is necessary to include quantum mechanics and the corpuscular nature of light. During the photoelectric effect, the electron in the shell of an atom absorbs the full energy of a γ quantum. This leads to the liberation of the electron from the atomic shell, while the rest of the absorbed energy becomes the kinetic energy of the electron. If the electron absorbs only part of the γ quantum energy, its binding energy is usually not exceeded, and the electron cannot leave the atomic shell. Thus, it is considered that only absorption of full γ quantum leads to electron emission. Fig. 3.1 shows that the photoelectric effect takes place mainly in the low-energy region of the measured γ spectrum.

3.1.2 Compton scattering

The Compton scattering is another manifestation of the particle behavior of photons, which occurs in the central region of the energy spectrum (Fig. 3.1). The γ photon scatters incoherently on an electron, loses part of its energy, which is transferred to the electron. After the interaction, the energy of the scattered γ particle is

$$E_{\gamma'} = \frac{E_\gamma}{1 + \frac{E_\gamma}{m_e c^2}(1 - \cos\theta)}, \tag{3.1}$$

where $m_e c^2$ is the rest energy of the electron and θ is the scattering angle. Thus, the energy of scattered electrons depends on the scattering angle. γ rays are in the energy range from tenths to units of MeV. For Compton scattering, the energy γ is much higher than the binding energy of the electrons, and the electrons are considered to be free and stationary.

3.1.3 Production of pairs of electron-positron

This phenomenon occurs if a high-energy photon interacts with the Coulomb field of the nucleus. The photon energy is converted into the rest masses of created particles. The threshold energy is $2m_e c^2$, i.e., 1.022 MeV (Fig. 3.1). The impact of this effect on the shape of the final spectrum is in Fig. 3.2.
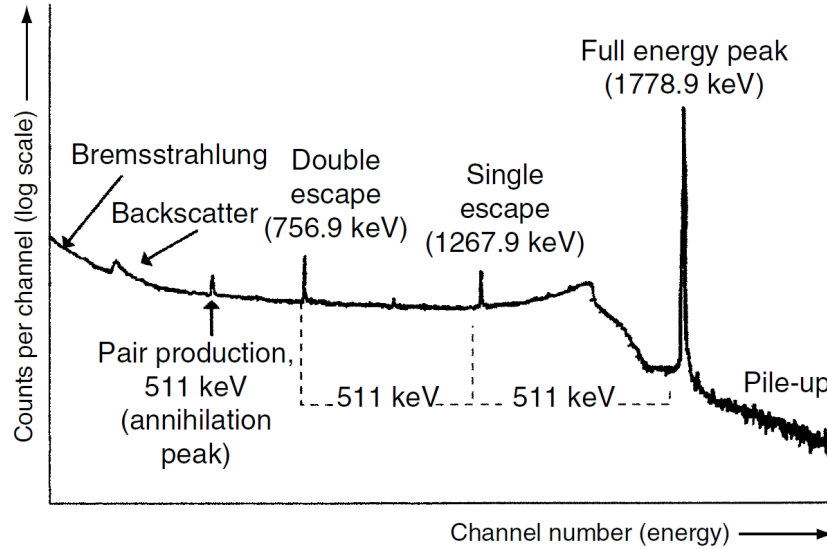
Fig. 3.2: Some of the aspects of γ spectra [77].

3.1.4 Interaction within the detector

The γ photon transfers a part or whole energy to the electron of the germanium atom. To conduct the electric signal, this electron has to create the electron-hole pair, which leads to the electric signal, which can be processed. There are a lot of other effects which contribute to the final signal, such as the size of the detector, the effect of the detector shielding, temperature of the detector, etc.

3.1.5 Data acquisition

The amount of absorbed γ ray energy is proportional to the electrical output of the detector, which is converted into the voltage pulse. This is amplified to be sorted by the multichannel analyzer (MCA). Each pulse is assigned to the channel according to the amplitude of the pulse. The relationship between the channel and the corresponding energy is linear. The time that takes for MCA to measure and process the incoming signal is called the dead time t_{dead} and it increases with the number of signals incoming to the MCA. It can be also expressed as the ratio between the real time of the measurement t_{real} and the time when the detector was active, live time t_{live}. The PC usually collects the data using the appropriate software.

The conversion between the numbers of channels and the corresponding energy is done by the energy calibration. This can be done by measuring the spectra of sources γ with well-known and separated γ lines, such as ^{22}Na, ^{60}Co, ^{137}Cs, etc. These spectra have typically one or two main peaks, which energies are well described. An example of the resultant spectrum is in Fig. 3.3
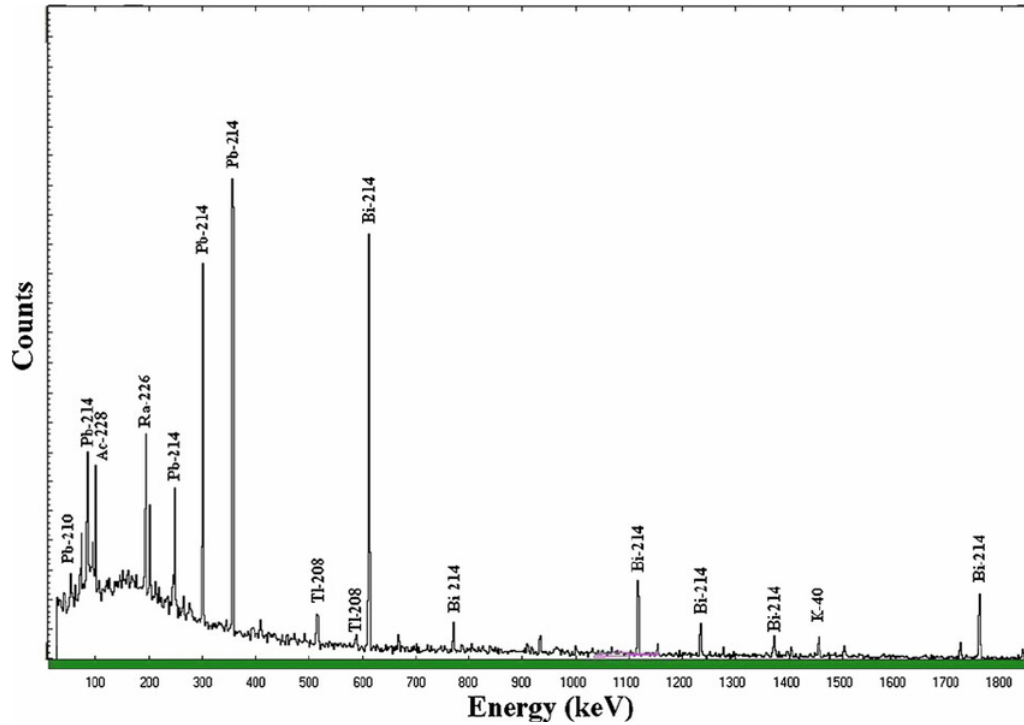
Fig. 3.3: Example of a spectrum of background natural radiation measured by the HPGe detector [79]

.

3.1.6 Estimation of the peak area

Further analysis is necessary to obtain information about the number of counts in each peak in the spectrum, which could correspond to the decay of an isotope of interest. The Deimos software [80] was used to estimate this number, which will be referred to as the peak area $S(E)$. The $S(E)$ is calculated from the fit of the measured data using the non-linear least squares method. The peak is fitted with a Gaussian function, which is the most suitable for HPGe spectroscopy. The information about the measurement parameters and about every evaluated peak is stored in a text file.

3.2 Corrections

The cross section can be estimated from the production rate Q which expresses the number of isotopes produced in the irradiated sample per one second. It is necessary to introduce several corrections to estimate the value of Q. These corrections are usually dependent on a large number of factors, i.e. γ energy, a parent isotope, the time between individual steps of the measurement, etc. The whole procedure for

calculating the production rate is described with individual steps of the evaluation process.

3.2.1   Radioactive decay

The number of radioactive products of the neutron interaction at time t is given by the equation

$$N(t) = N_0 e^{-\lambda \cdot t}, \tag{3.2}$$

where N_0 is $N(t)$ for the time $t = 0 \, \text{s}$ and λ is the decay constant of the radioactive isotope.

Since the start of the irradiation starts also the decay of the radioactive products. The first decay interval which has to be corrected is the decay during irradiation. The correction takes the form

$$\frac{\lambda}{1 - e^{-\lambda \cdot t_{irr}}}, \tag{3.3}$$

where t_{irr} is the duration of the irradiation.

The decay between the end of the irradiation and the beginning of the measurement t_{delay} causes another decrease in the number of measurable counts. This is expressed by

$$\frac{1}{e^{-\lambda \cdot t_{delay}}}. \tag{3.4}$$

The last interval for which is necessary the correction is the time of the measurement:

$$\frac{1}{1 - e^{-\lambda \cdot t_{real}}}. \tag{3.5}$$

3.2.2   Full-energy peak efficiency of the detector

The full-energy peak (FEP) efficiency $\varepsilon_{FEP}(E_\gamma)$ describes the ability of HPGe to detect a gamma photon of a certain energy. To estimate $\varepsilon_{FEP}(E_\gamma)$ calibration detectors are usually used, such as ^{60} Co, ^{152} Eu, etc. For the peaks of the measured spectrum are calculated $\varepsilon_{FEP}(E_\gamma)$ from the equation

$$\varepsilon_{FEP}(E_\gamma) = \frac{S(E_\gamma) \cdot \lambda \cdot e^{\lambda t_0}}{A_0 \cdot I_\gamma(E_\gamma) \cdot (1 - e^{-\lambda t_{real}})} \frac{t_{real}}{t_{live}}, \tag{3.6}$$

where t_0 is the time when the reference activity A_0 of the calibration sample was estimated. $I_\gamma(E_\gamma)$ is the intensity of the peak at the given energy. If the results for individual energies are fitted with polynomials, the FEP efficiency curve can be constructed. Its typical shape is in Fig. 3.4 The efficiency calibration is necessary to compare the peaks in individual parts of the spectrum.
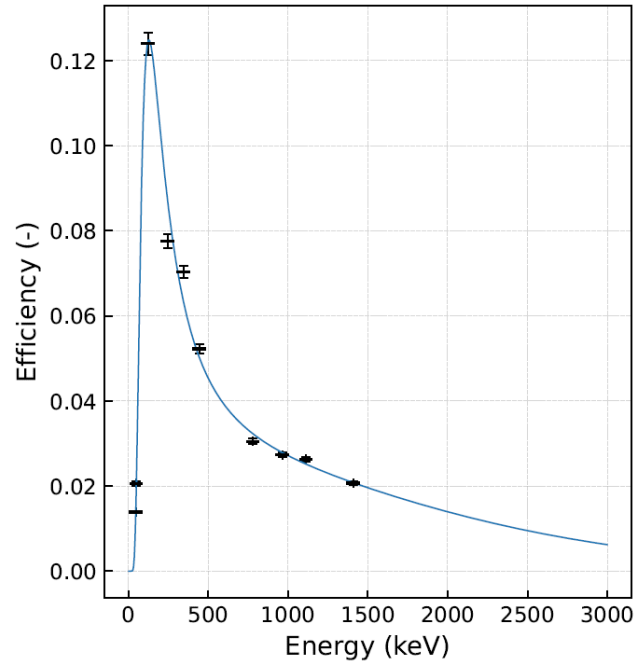
Fig. 3.4: Measured data and their fit for estimation of the FEP efficiency.

3.2.3 Nonlinearity of the detector

The Deimos software uses linear energy calibration to assign the correct energy to the number of channels. However, the dependency is not exactly linear and this simplification introduces an uncertainty into the measurement which can be as observed as a difference between measured and theoretical values. Such a phenomenon is problematic since the shift of the peak can cause it not to be recognized. Thus, it
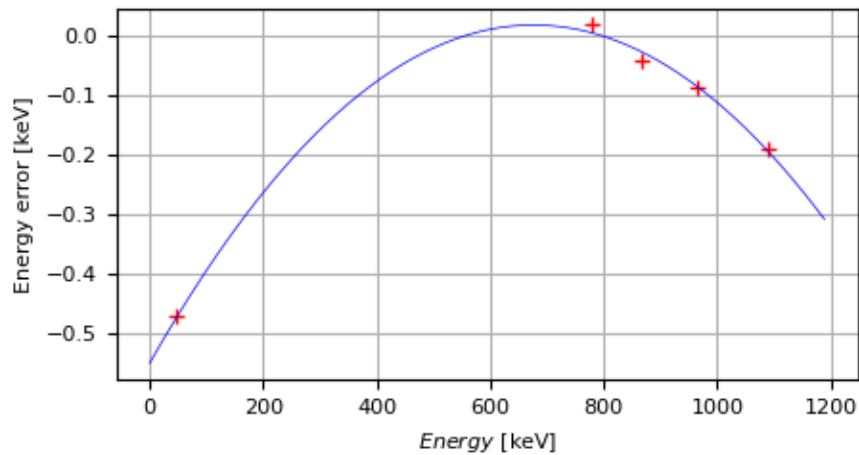
Fig. 3.5: The nonlinearity curve.

is appropriate to introduce the correction for nonlinearity C_{nlin}. It is done by calculation of differences between measured and theoretical values of energies of peaks of calibration detectors. These differences can be fitted with a polynomial of the second order, resulting in a nonlinearity curve (Fig. 3.5), from which it is possible to derive true values in the whole spectrum.
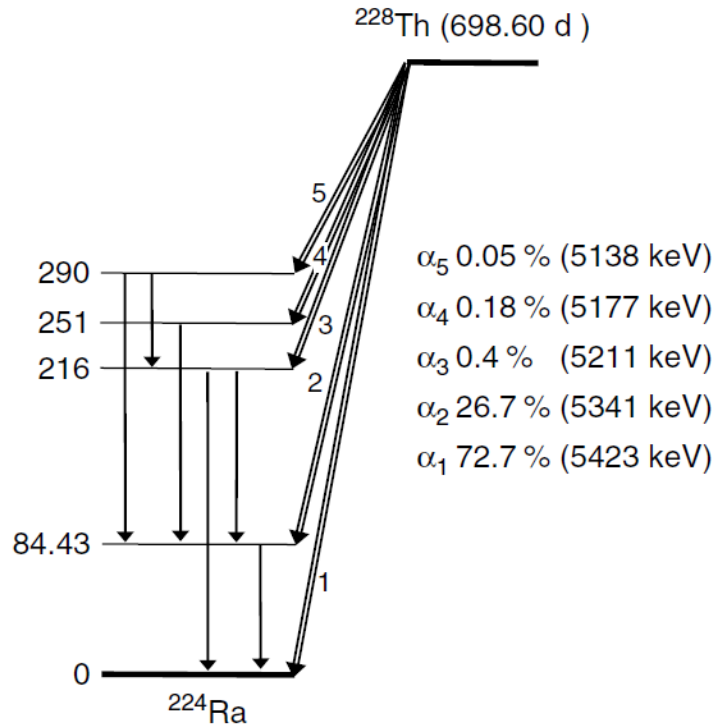
Fig. 3.6: An example of the various levels of decaying nucleus (for thorium) [77].

3.2.4 True cascade coincidences

Radioactive decay is not always straightforward. Instead, the final (ground) state can be produced via different decays. An example in in Fig. 3.6. Thus, the electric signal processed by MCA can be caused, for example, by one photon with energy X or by two photons with energies Y + Z = X (the principle is visualized in Fig. 3.7). This effect takes place mainly if the position of the measured sample is close to the detector. For higher distances the true cascade coincidences are negligible. The correction is marked COI_E and depends on the isotope and the geometry of the measurement. To calculate correction factors the software uses TrueCoinc software [82].
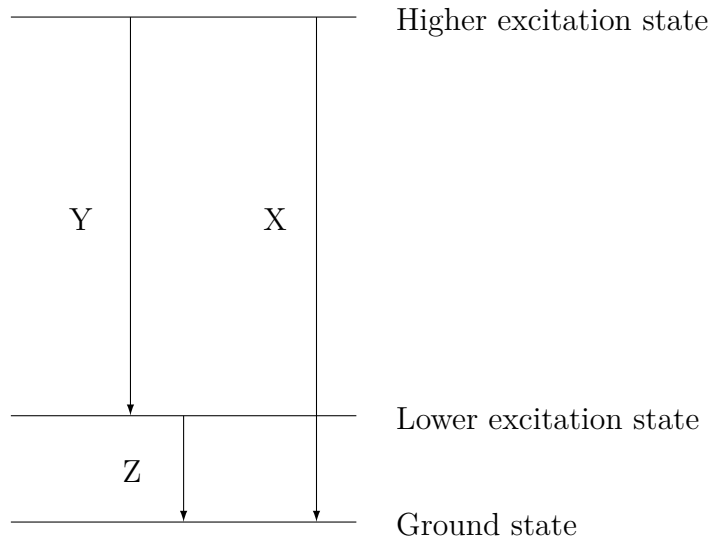
Fig. 3.7: True cascade coincidences principle.

3.2.5 Self-attenuation

In reality, the measured sample has a thickness, which is not negligible. This leads to attenuation of some of the emitted γ photons in the material of the sample. The ability of the sample to attenuate the gamma photon depends on its energy, the density of the material, and the thickness of the sample. The correction factor C_{att} is given by the equation

$$C_{att} = \frac{h \cdot \mu \cdot \rho}{1 - e^{h \cdot \mu \cdot \rho}}, \tag{3.7}$$

where h is the thickness of the sample, μ is the attenuation coefficient and ρ is the density of the material of the sample.

3.2.6 Background

The signal coming to the detector is not caused only by isotopes in the measured sample. The impact of the surrounding environment can be significant for some energies. To subtract the signal from the background is used the correction C_{bcg}

$$C_{bcg} = \frac{t_{live}}{t_{live,bcg}} S(E_{\gamma,bcg}). \tag{3.8}$$

Elements of the equation with the lower index *bcg* are taken from the measurement of the background.

3.3 Production rate

After the application of C_{nlin} on the measured energy and the application of C_{bcg} on the measured area, the production rate for selected gamma energy can be now expressed by the equation

$$Q(E_\gamma) = S(E_\gamma) \frac{t_{real}}{t_{live}} \frac{1}{I_\gamma(E_\gamma)} \frac{e^{\lambda t_{delay}}}{1 - e^{-\lambda t_{real}}} \frac{\lambda}{1 - e^{-\lambda t_{irr}}} \frac{C_{att}}{\varepsilon_{FEP}(E_\gamma)COI_E}, \qquad (3.9)$$

where $I_\gamma(E_\gamma)$ is intensity of the peak of interest.

Spectra of produced isotopes are often complex with a large number of peaks. In the case when more than one value of production rate is estimated for the produced isotope, the final production rate is calculated as the weighted average

$$Q = \frac{\sum_{i=1}^{n} w_i \cdot Q(E_{\gamma,i})}{\sum_{i=1}^{n} w_i}, \qquad (3.10)$$

where the weight of the i-th contribution w_i is

$$w_i = \left(\frac{1}{dQ(E_{\gamma,i})} \right)^2, \qquad (3.11)$$

and $dQ(E_{\gamma,i})$ is an uncertainty of the production rate calculated for ith gamma energy peak.

3.4 Contribution of isomeric states

The isotope of interest is not always produced exclusively from one parent isotope. For example, in the case of neutron interaction with ^{197}Au can be produced ^{196}Au directly, or via decay of another product of the interaction, ^{196m}Au. It was chosen the different approach to estimate the production rate from the original parent isotope, according to [81]. These two states are distinguished on the basis of different $T_{1/2}$, thus the decay between individual steps of measurement. In following equations is g for the ground state and m for the isomeric state of the isotope.

3.4.1 Decay during cooling and measurement

The production rate of the isomeric state after irradiation would be

$$Q_{m0} = S_m \frac{t_{real}}{t_{live}} \frac{1}{I_{\gamma,m}} \frac{e^{\lambda_m t_{delay}}}{1 - e^{-\lambda_m t_{real}}} \frac{C_{att}}{\varepsilon_{FEP}COI_E}, \qquad (3.12)$$

and the production rate of the ground state after irradiation would be

$$Q_{g0} = S_g \frac{t_{real}}{t_{live}} \frac{1}{I_{\gamma,g}} \frac{e^{\lambda_g t_{delay}}}{1 - e^{-\lambda_g t_{real}}} \frac{C_{att}}{\varepsilon_{FEP}COI_E} + \frac{\lambda_m Q_{m0}}{\lambda_g - \lambda_m} \left(1 - e^{(\lambda_g - \lambda_m)t_{delay}} \right). \qquad (3.13)$$

3.4.2 Decay during irradiation

The correction for decay during irradiation is

$$C_{g,irr} = \frac{\lambda_g t_{irr}}{1 - e^{-\lambda_g t_{irr}}} - \frac{Q_m}{Q_{g0}(1 - e^{-\lambda_g t_{irr}})}\left(1 - \frac{\lambda_m e^{-\lambda_g t_{irr}} - \lambda_g e^{-\lambda_m t_{irr}}}{\lambda_m - \lambda_g}\right), \quad (3.14)$$

where Q_m is calculated from Eq. 3.10. Final production rate of the ground state is

$$Q_g = Q_{g0}C_{g,irr}. \quad (3.15)$$

3.5 Neutron background subtraction

The spectra of produced neutrons are not exactly mono-energetic. A non-negligible fraction of the total neutron flux consists of background neutrons with lower energy. A non-negligible amount of these neutrons is produced by reactions in the carbon stopped, which is a part of the experimental setup. These neutrons can be observed as a background in the low-energy part of spectra next to the main peak. In Fig. 3.8 are neutron fluxes calculated in MCNP compared to cross-sections calculated in TALYS. To estimate cross-section within the given energy, the contribution
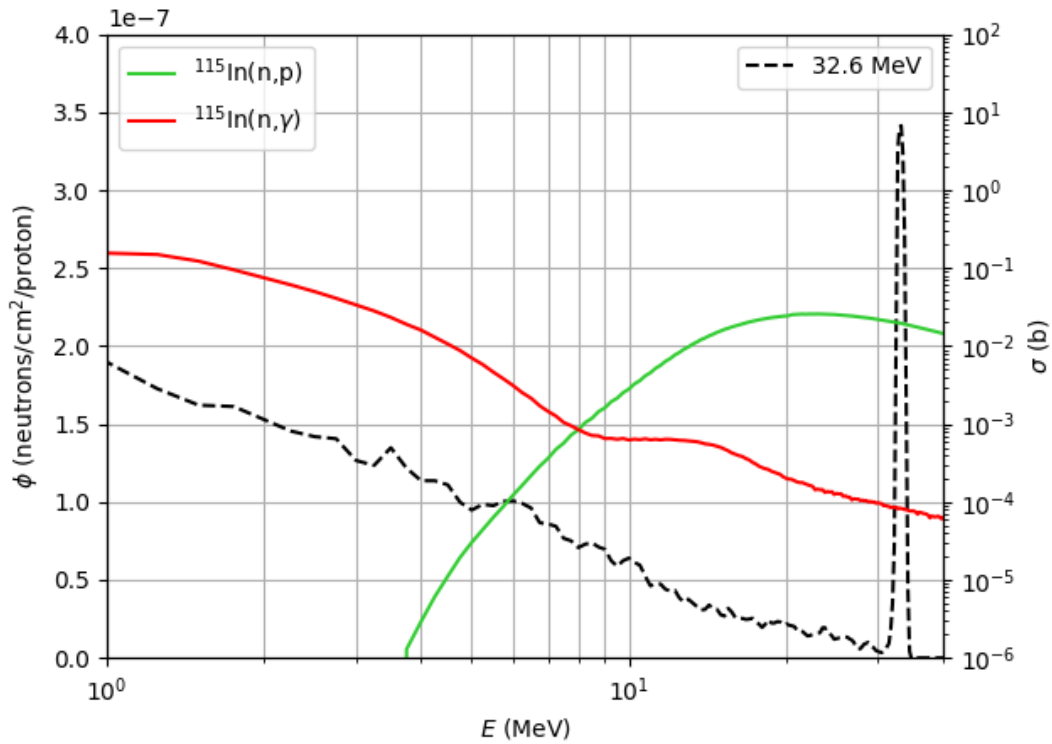

Fig. 3.8: Comparison of neutron flux (black) to cross-sections of various reactions.

of neutrons from background has to be subtracted. The method is described in [83]. The subtraction is done by the folding of neutron spectra and cross-section of the observed reaction. The values are estimated from simulations (neutron flux from MCNP and cross-sections from TALYS) and the calculation supposes the same step of energy bins. The correction for the neutron background subtraction has a form

$$C_{n,bcg} = \frac{\sum_i \sigma_i N_i}{\sum_j \sigma_j N_j}, \tag{3.16}$$

where N is neutron fluence. Index i stands for bins belonging to the peak, j is for the whole spectrum. It is possible to subtract the neutron background experimentally, by measurement of cross-sections step-by-step in small energy intervals [84]. This method decreases the uncertainty of the process, however, it is difficult to measure all of the necessary data. Another method is to irradiate foils off the axis of the direction of neutrons. These are irradiated only by background neutrons, thus the background can be subtracted through the difference between production rates.

3.6 Cross-sections estimation

The final value of the cross-section of the reaction is given by the formula

$$\sigma = \frac{QSC_{bg}}{\frac{N_n}{t_{irr}} \frac{N_A m_r}{A_r}}, \tag{3.17}$$

where S is the area of the foil perpendicular to the direction of the proton beam, N_n is the neutron fluence, t_{irr} is the duration of the irradiation, N_A is the Avogadro constant, m_r is the weight of the foil and A_r is the relative atomic mass.

3.7 Estimation of neutron fluence

There are several methods to estimate neutron fluence. For example, during the irradiation, the isotopes of the lithium target are activated by incoming protons and this interaction leads to the creation of radioactive beryllium. After the end of the irradiation, the activity of the target is measured and the neutron fluence is calculated.

For this thesis was chosen another approach. The method takes advantage of the fact that some isotopes have well-measured microscopic cross-sections. Such isotope can be ^{197}Au. The other advantage of gold is, that the isotope 197 has 100 % abundance in the natural gold. For this method, the foil is irradiated together with the foil of the interest of the measurement. Production rates are evaluated in the

same way as for the estimation of cross-sections. The neutron fluence is expressed from 3.17 and calculated as

$$N_n = \frac{QSC_{bg}}{\frac{\sigma}{t_{irr}} \frac{N_A m_r}{A_r}}. \qquad (3.18)$$

3.8 Software

The estimation of cross-sections includes a large number of calculations. These are often complicated and not straightforward. Furthermore, manual calculation can be a source of error. Some of the necessary steps (such as the simulation of neutron flux) require special software. Following programs were used for calculations described in this thesis.

3.8.1 Software for evaluation of production rates

A new software [85] was developed at FEEC to simplify the process of application of individual corrections. Originally, the software was designed to calculate reaction rates and create the input file for SAND-II. The software was improved during the work on this thesis with the aim of calculating of the final production rates according to the equations which were described above. The input for the software are data files from software Deimos. The software also has modules for the creation of necessary libraries, e.g., the library for nonlinearity or FEP efficiency.

3.8.2 MCNP

Monte Carlo N-Particle (MCNP) code is a multipurpose code for the simulation of particle transport. The user provides an input file, with the specification of the geometry of inspected set-up, used materials, nuclear data libraries, and monitored data. For this thesis was used the version MCNP6.2 to simulate the experimental set-up - the lithium target irradiated with protons. The neutron flounce was monitored in cells of indium and gold foils via tally F4 which provides information about average neutron flux in cell.

3.8.3 TALYS

TALYS is the software for the simulation of nuclear interactions up to the energy of 200 MeV. It allows users to generate nuclear data for further application with a simple input file, which specifies the isotope of interest. The version TALYS1.4 was used to simulate cross-sections of observed interactions.

4 Results

Three experiments were conducted at INR Řež in 2019 at cyclotron U-120M, which is a part of the CANAM infrastructure. The experiments were carried out by Dušan Král, the supervisor of this thesis.

The quasi-monoenergetic neutron source was the lithium target irradiated with a proton beam. Proton energies in individual experiments were 20 MeV, 31.5 MeV, and 35.5 MeV, which led to neutron energies 17.6 MeV, 30.6 MeV, and 32.6 MeV, respectively. During experiments were irradiated stocks of foils from various materials. Radioactive products of neutron interactions in separate foils were measured at five different HPGe detectors located at Řež, Vyškov, and Brno. Tab. 4.1 summarises information about irradiation and indium samples. It was used the natural indium with abundances 95.7 % of ^{115}In and 4.3 % of ^{113}In.

Tab. 4.1: Energy of protons and neutrons, the irradiation time, weight, and area of irradiated indium samples in individual experiments.

Experiment	E_p (MeV)	E_n (MeV)	t_{irr} (min)	m (g)	S (cm^2)
1	32.5	30.6	474.167	0.1142	2.5×2.5
2	35.5	32.6	797.0	0.1176	2.5×2.5
3	20.0	17.6	714.0	0.1142	2.5×2.5

Measured data were evaluated in the Deimos software, where were estimated areas of peaks in individual spectra. The results of the computation of production rates are summarized in Tab. 4.2.

Tab. 4.2: Production rates for products of individual reactions.

Reaction	E=17.6 MeV Q (1/s)	E=30.6 MeV Q (1/s)	E = 32.6 MeV Q (1/s)
^{nat}In(n,x)^{114m}In	27263 ± 1339.4	46683 ± 6683.3	57130 ± 11883
^{115}In(n,n')^{115m}In	9801.7 ± 2034.4	31460 ± 217.95	45561 ± 9764.8
^{115}In(n,γ)^{116m}In	556.8 ± 377.21	1388.2 ± 550.87	147.45 ± 1088.9
^{115}In(n,p)^{115}Cd	120.92 ± 4.1879	614.77 ± 9.4122	557.47 ± 8.9271
^{115}In(n,α)^{112}Ag	105.89 ± 11.421	319.38 ± 29.542	357.61 ± 94.903
^{115}In(n,3n)^{113m}In	421.74 ± 69.953	6187.5 ± 42.72	6929.4 ± 1459.8
^{113}In(n,α)^{110m}Ag	-	12.698 ± 1.15	1245.2± 408.72
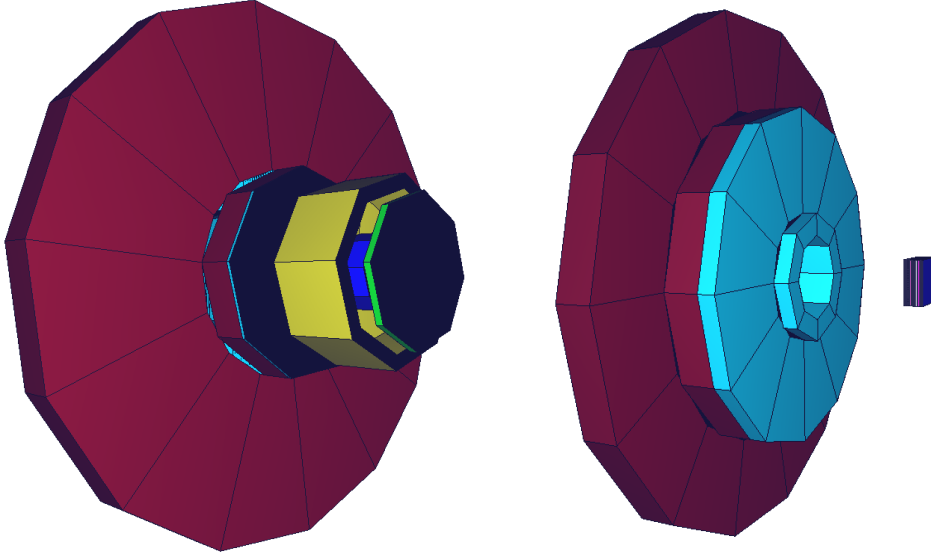
Fig. 4.1: 3D model of the geometry input for MCNP simulation. On the left is the view from the source of protons, and on the right is the sandwich of irradiated foils.

The experimental set-up was simulated in MCNP6.2 to determine neutron fluences. As input was used M. Majerle's model of the lithium target (see Fig. 4.1). The original input file had to be modified for version 6.2. The simulation run for $1 \cdot 10^9$ source particles to decrease the uncertainty. The tally F4 was used to monitor the neutron fluence in cells. Resultant fluences in indium foils are plotted in Fig. 4.2. Cross-sections of individual neutron reactions were evaluated using TALYS1.4. The background subtraction was done using these data. Its values are in Tab. 4.3 together with half-lives of observed isotopes. The data show the decrease of the value

Tab. 4.3: Half-lifes and background corrections for individual products of neutron interactions with indium foil.

		E=17.6 MeV	E=30.6 MeV	E = 32.6 MeV
Reaction	$T_{1/2}$	C_{bcg}	C_{bcg}	C_{bcg}
^{nat}In(n,x)^{114m}In	49.51 d	0.792	0.312	0.242
^{115}In(n,n')^{115m}In	4.486 h	0.082	0.050	0.038
^{115}In(n,γ)^{116m}In	54.29 m	0.004	0.001	0.0007
^{115}In(n,p)^{115}Cd	53.46 h	0.861	0.664	0.583
^{115}In(n,α)^{112}Ag	3.13 h	0.965	0.582	0.465
^{115}In(n,3n)^{113m}In	99.476 m	1	0.852	0.672
^{113}In(n,α)^{110m}Ag	249.83 d	-	0.470	0.352

of the background correction with an increase of the peak neutron energy. This is caused either by the decrease of cross-sections in the region of higher energies and by the increase of the amount of background neutrons which contributes to the number of interactions. These statements are shown in Fig. 4.2.
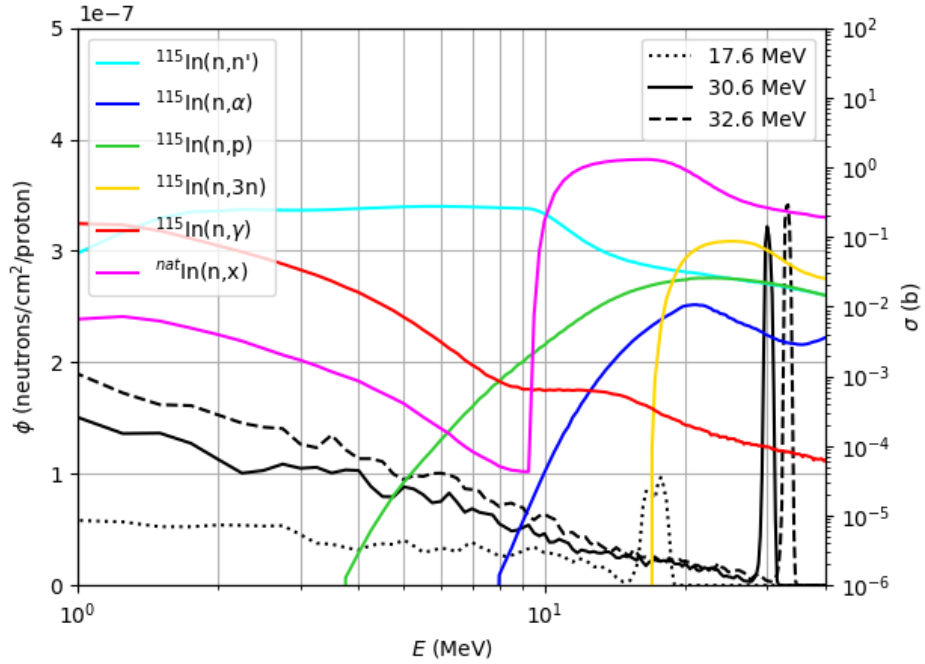
Fig. 4.2: Comparison of neutron fluxes in all three experiments (black) to cross-sections of various reactions (colors).

Final cross sections were calculated after all previously mentioned steps. Results are summarized in Tab. 4.4. Results are graphically compared with evaluated cross-section data from libraries ENDF/B-VIII.0 [76], JENDL-5 [86] and TENDL-2019.s90 [87] and with data from EXFOR database [88]. The libraries were selected based on the range of available energies. All of libraries used for comparison, except of ENDF/B-VIII.0, claims to be evaluated up to energies higher than 32.5 MeV, the highest neutron peak enegy during experiments. However, for some reactions, the data are not available.

Tab. 4.4: Calculated cross-sections.

Reaction	E=17.6 MeV σ (b)	E=30.6 MeV σ (b)	E = 32.6 MeV σ (b)
^{nat}In(n,x)^{114m}In	0.7695 ± 0.1152	0.2996 ± 0.06029	0.1774 ± 0.0446
^{115}In(n,n')^{115m}In	0.0288 ± 0.0072	0.0326 ± 0.0046	0.0225 ± 0.0058
^{115}In(n,γ)^{116m}In	0.07e-3 ± 0.05e-3	0.03e-3 ± 0.01e-3	0.001e-3 ± 0.01e-3
^{115}In(n,p)^{115}Cd	0.0037 ± 0.0005	0.0084 ± 0.0012	0.0042 ± 0.0006
^{115}In(n,α)^{112}Ag	0.0036 ± 0.0006	0.0038 ± 0.0006	0.0021 ± 0.0006
^{115}In(n,3n)^{113m}In	0.0150 ± 0.0033	0.1085 ± 0.0154	0.0599 ± 0.0152
^{113}In(n,α)^{110m}Ag	-	0.00012 ± 0.00002	0.0056 ± 0.0020

Cross-sections in Fig. 4.3 are calculated for natural indium. Both isotopes of natural indium can produce ^{114m}In thus the final values are composed of contributions of reactions (n,2n) and (n, γ) on ^{115}In and ^{113}In, respectively. However, as the graph in Fig. 4.3 shows, the contribution from the ^{113}In(n, γ) reaction is three orders lower than the contribution of ^{115}In(n,2n). Also the isotopic abundance of ^{115}In is significantly higher (95.7 %). Thus, it is possible to assume that most of the measured reactions were from (n,2n). TALYS simulated the neutron interaction
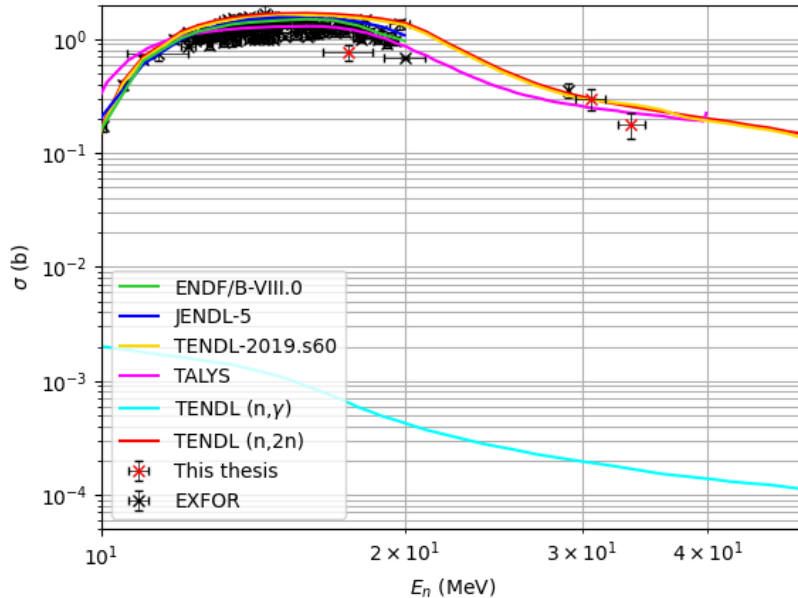
Fig. 4.3: Calculated cross-sections of ^{nat}In(n,x)^{114m}In reaction compared to evaluated data.

with ^{nat}In. The results are compared to cross-sections for individual contributing reactions and to data from the EXFOR database for the reaction ^{115}In(n,2n).

Fig. 4.4 shows the cross-sections for the production of the isotope ^{115m}In. The result for 17.6 Mev is shifted compared to data from TENDL library. Considering the fact that the contribution of neutrons from the quasi-monoenergetic peak was only 8 % (Tab. 4.3), the results are acceptable.
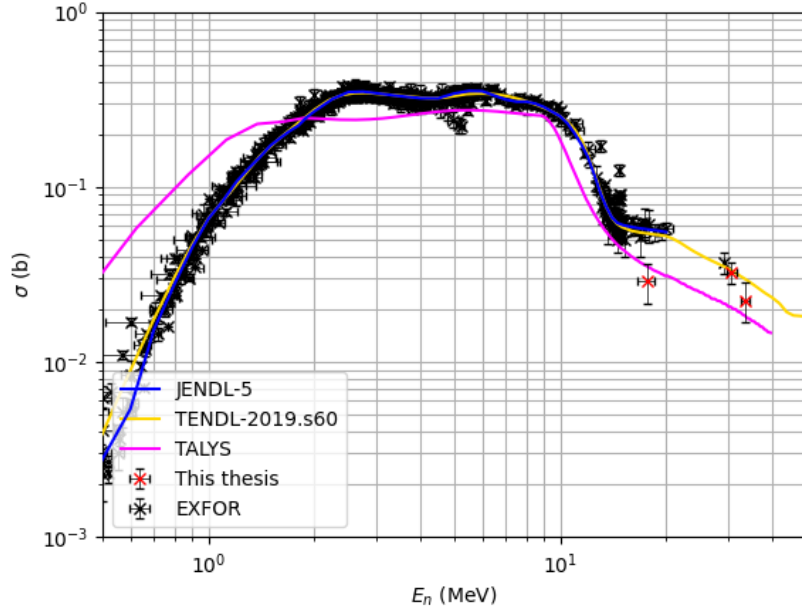
Fig. 4.4: Calculated cross-sections of ^{115}In(n,n') reaction compared to evaluated data and EXFOR.

The complication connected to the neutron background is possibly also the cause of the shift of results in the case of ^{115}In(n,γ). As was shown in Fig. 4.2, for some reactions, as for this one, the contribution of background neutrons is larger than that of neutrons from the quasi-monoenergetic peak. Tab. 4.3 shows that this effect was the most important in the case of ^{115}In(n,n') (Fig. 4.4) and ^{115}In(n,γ) (Fig. 4.5). Almost 100 % of ^{115}In(n,γ) interactions were caused by background neutrons. Another reason can be a small amount of measured data (especially in the case of measurement after a longer time).

Fig. 4.5: Calculated cross-sections of ^{115}In(n,γ) reaction compared to evaluated data and EXFOR.
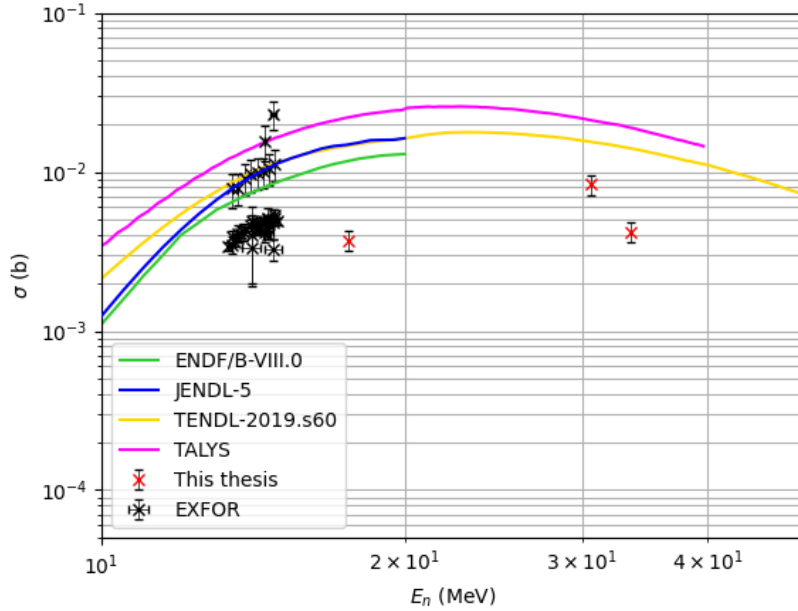
Fig. 4.6: Calculated cross-sections of ^{115}In(n,p) reaction compared to evaluated data and EXFOR.

Fig. 4.6 shows data for the reaction ^{115}In(n,p). It shows that measured data does not properly correspond to the evaluated data from libraries and their shift is

probably systematic. The reason could be, that ^{115}Cd, the product of this reaction, deexcites through the same γ line as ^{115m}In, which is a product of ^{115}In(n,γ) reaction. It is also shown the lack of data in the higher energy range, even for reactions that are well measured in the lower energy region.
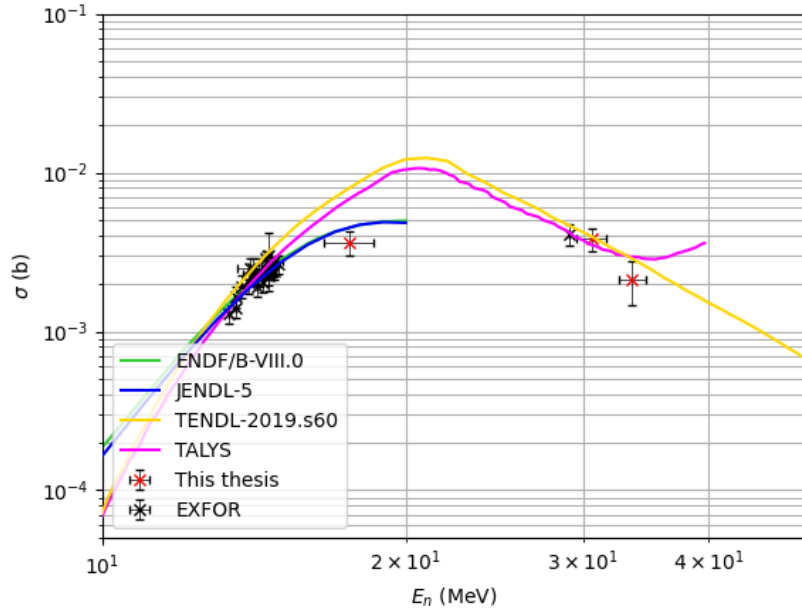
Fig. 4.7: Calculated cross-sections of ^{115}In(n,α) reaction compared to evaluated data and EXFOR.

The data in Fig. 4.7 fits to the evaluated data the best among the results in this work. also for this reaction is measured large amount of data, but in lower energy region. In the energy region of interest of experiments described in this work are experimental data missing for all reactions on indium. Another example of data that are approaching evaluated values is in Fig. 4.8.

On contrary, values calculated for reaction ^{113}In(n,α) in Fig. 4.9 differ a lot from data from libraries. This could be caused by the low abundance of the ^{113}In in the natural indium.
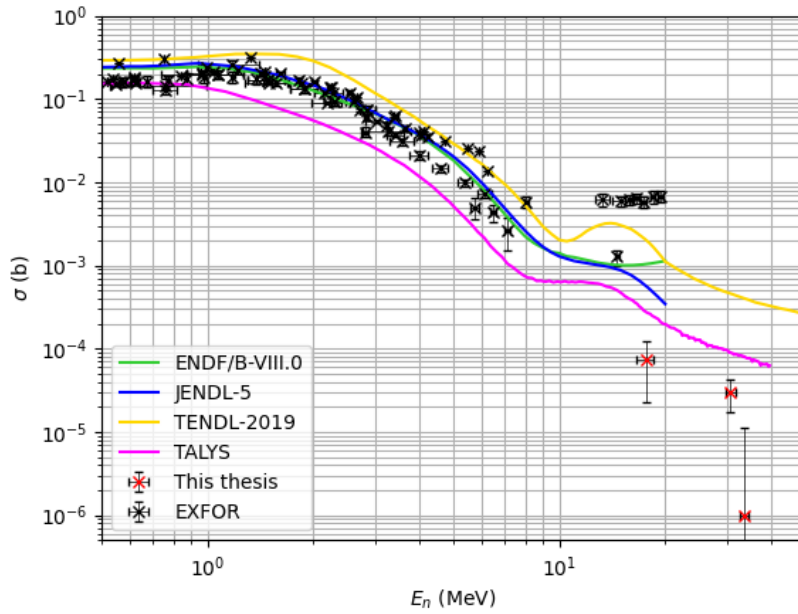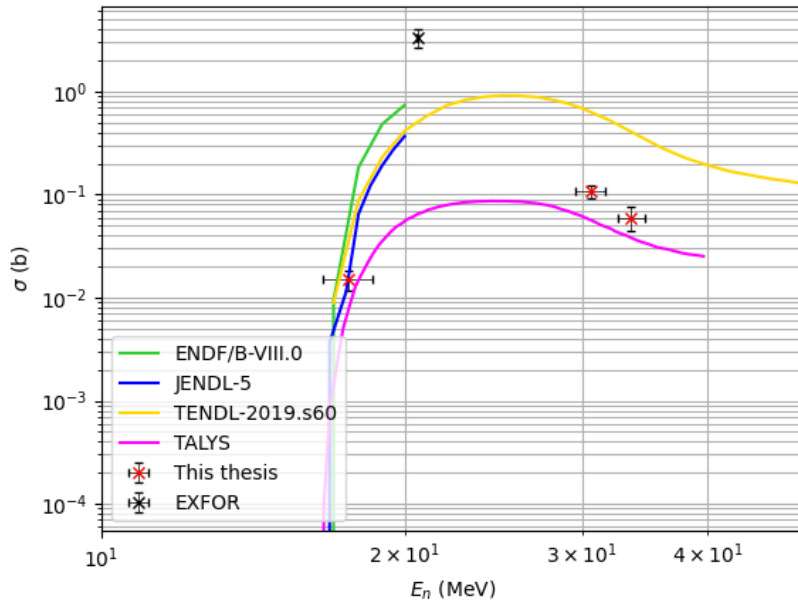
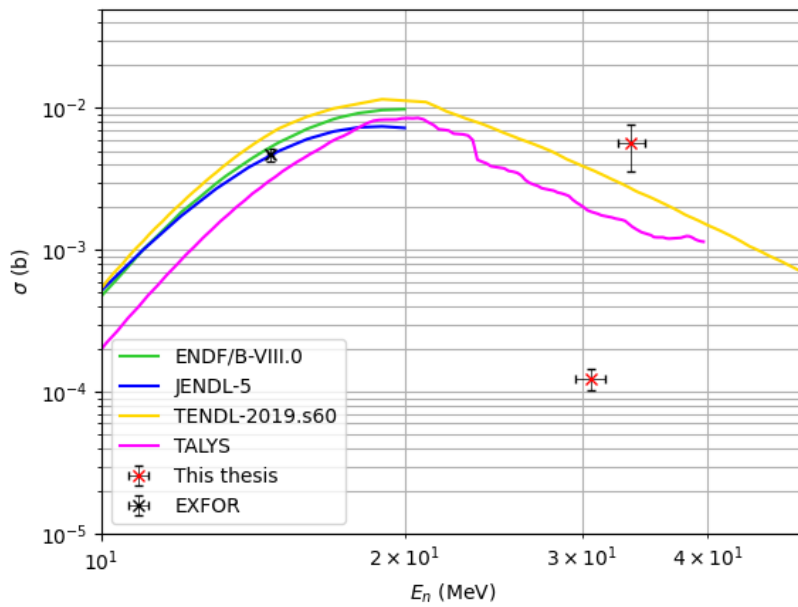Fig. 4.8: Calculated cross-sections of ^{115}In(n,3n) reaction compared to evaluated data and EXFOR.

Fig. 4.9: Calculated cross-sections of ^{113}In(n,α) reaction compared to evaluated data and EXFOR.

Conclusion

Neutrons are important tools for many fields of science, medicine, and industry. For their adequate use, it is necessary to determine their purpose and according to this design an appropriate source. It was shown that there are many possibilities of neutron production. The selection depends on the required neutron flux and energy. Radioisotopic neutron sources are the most widely used, due to their price and relative ease of use. However, there is an effort to replace them with neutron generators.

The information in the previous text implies that there is a risk of lack of accessibility of neutron beam time in the future. This could be caused by the shut down of aging research reactors. However, the development of spallation sources (such as ESS in Sweden) together with CANS (i.e., German HBN) and commercially available neutron generators offers promising prospects. As an advantage appears the combination of high neutron flux of spallation sources and lower neutron flux of CANS. This will allow researchers to choose the source right according to their needs.

A lot of projects are focused on improving targets for neutron production. New targets should be more durable and they should produce neutrons with more convenient characteristics.

It was also shown that the result of neutron interaction relies on its energy and the type of target nucleus. The probability that a reaction occurs can be described by its cross-section. The meaning of cross-sections and the principle of the measurement was briefly introduced.

In the practical part of the thesis were evaluated data from the measurement of microscopic cross-sections of indium. It was used the quasi-monoenergetic neutron source to get the most accurate neutron energy. It was used the lithium source irradiated with protons. However, even in the case of a real neutron source, the neutron spectrum consists not only of the mean neutron peak but is has also a characteristic neutron background, which increases with the decreasing neutron energy. Data were evaluated for three experiments, which were the same in setup, but differed in the energy of used protons, thus in the neutron peak energy. The products of neutron reactions were measured with the HPGe detector.

It was described the process of data acquisition and processing from the interaction of photons to the calculation of the final microscopic cross-sections. For part of this process, namely for the calculation of production rates of individual isotopes, was used the software developed at FEEC. The software was adjusted for this type of calculation. In addition, the functionality of the software was tested. The values evaluated from measurement were compared to cross-sections from three libraries of

evaluated data and EXFOR database.

A significant amount of uncertainty has to be considered. Some of them are given by the character of the detection of γ rays. The HPGe detector is very sensitive for electromagnetic noise. Even without noise, the efficiency of detection is maximal in a relatively small range of energies and then rapidly decreases. There are also other influences, such as the decay rate of products of reactions or parameters of the sample itself (isotopic purity, thickness, etc.).

The other important source of uncertainty is the method of subtraction of the neutron background. In this thesis was chosen the method based on simulations of the neutron flounce and the reaction cross-sections. The role of chosen libraries for calculations is significant. It exists also an experimental method but there are no data for its application in this thesis.

Since the decay scheme of the isotope of interest is often complicated, the reason of the deviation of the data from the expected value can be also caused by a wrong estimation of levels, between which the transition took place. Some γ energies for different transitions or even for different isotopes are similar and is is difficult to distinguish the origin of the γ photon production.

Considering all these sources of uncertainties, the final results show that a lot of evaluated data approaches theoretical values, e.g., for reaction ^{115}In(n,α). The largest deviation from expected values was observed for ^{113}In(n,α), where the parent isotope has a low abundance in the natural indium; for ^{115}In(n,γ) due to the non-negotiable influence of background neutrons, and for ^{115}In(n,p) where the deviation appears systematic and could be caused by the wrong estimation of the appropriate γ line. In future it should be considered to choose another method of estimation of the correction for the neutron background to increase the precision of the evaluation. It would be also interesting to observe the behavior of the value of the correction depending on the selection of the source of cross-section data. The problem of the γ lines with similar energies could be solved in the future by comparison with other peaks in the spectrum and their intensities. For the whole spectrum, the peak areas should be proportional to their intensities.

Bibliography

[1] TOLKIEN, J.R.R. *The Lord of the Rings* [online]. London: Harper-CollinsPublishers, 2005 [cit. 2022-05-19]. ISBN 978-0-06-191780-6. Available online: https://gosafir.com/mag/wp-content/uploads/2019/12/Tolkien-J.-The-lord-of-the-rings-HarperCollins-ebooks-2010.pdf

[2] JONES, Dave. *Global Electricity Review 2021: Global Trends* [online]. In: . EMBER, March 2012, s. 26 [cit. 2022-01-14]. Available online: https://apo.org.au/sites/default/files/resource-files/2021-03/apo-nid311621.pdf

[3] Neutrons and energy: Highlights of ILL research. *Neutrons for Science* [online]. ILL [cit. 2022-01-14]. Available online: https://www.ill.eu/fileadmin/user_upload/ILL/1_About_ILL/Documentation/Neutrons_and_energy_2015.pdf

[4] The Roles Of Radiation, Neutrons, And N-Ray In Medicine. *Phoenix: Transforming Nuclear Technology* [online]. Phoenix, LLC., 2022 [cit. 2022-01-14]. Available online: https://phoenixwi.com/neutron-generators/radiation-neutrons-n-ray-medicine/

[5] DAN. *NASA Science Exploration Program* [online]. [cit. 2022-05-19]. Available online: https://mars.nasa.gov/msl/spacecraft/instruments/dan/

[6] IAEA. *Neutron genera tors for analytical purposes* [online]. Vienna: IAEA, 2012 [cit. 2021-12-13]. IAEA Radiation Technology Reports Series, 1. ISBN 978-92-0-125110-7. Available online: https://www-pub.iaea.org/mtcd/publications/pdf/p1535_web.pdf

[7] *Paul Scher rer Institut* [online]. Switzerland: PSI, 2022 [cit. 2022-01-09]. Available online: https://www.psi.ch/en

[8] *Compact Accelerator Based Neutron Sources* [online]. IAEA, 2021 [cit. 2022-01-04]. ISBN 978-92-0-133221-9. IAEA TECDOC No. 198120. Available online: https://www-pub.iaea.org/MTCD/ Publications/PDF/TE-1981web.pdf

[9] FILGES, D. a F. GOLDENBAUM. *Handbook of Spallation Research: T heory, Experiments and Applications* [online]. 1. Wiley-VCH, 2010, 787 s. [cit. 2022-01-09]. ISBN 9783527628865. DOI:10.1002/9783527628865

[10] LEDOUX, X., M. AÏCHE, M. AVRIGEANU, et al. The neutrons for science facil ity at SPIRAL-2. *EPJ Web of Conferen ces* [online]. 2017, **146** [cit. 2022-01-09]. ISSN 2100-014X. DOI:10.1051/epjconf/201714603003

[11] CUBITT, Robert a Giovanna FRAGNETO. Neutron Reflection. *Scattering* [online]. Elsevier, 2002, 20 02, , 1198-1208 [cit. 2022-01-09]. ISBN 9780126137606. DOI:10.1016/B978-012613760-6/50065-6

[12] *S-DH: Neutron Guide News at S-DH* [online]. Heidelberg: S-DH, 2022 [cit. 2022-01-13]. Available online: https://www.s-dh.de/

[13] FANTIDIS, Jacob G, Bandekas V DIMITRIOS, Potolias CONSTANTI-NOS, Vordos NICK, M. SEDAGHAT, R. SABRI, B. POURSHAHAB a V. DAMIDEH. Fast and thermal neutron radiographies based on a compact neutron generator. *Journal of Theoretical and Applied Physics* [online]. 2012, **6**(1), 62-65 [cit. 2022-01-09]. ISSN 2251-7235. DOI:10.1186/2251-7235-6-20

[14] KENNETH S., Krane. *Introductory Nuclear Physics* [online]. 3rd. USA: John Wiley & Sons, 1988 [cit. 2021-12-13]. ISBN 978-0-471-80553-3. Available online: https://faculty.kfupm.edu.sa/PHYS/aanaqvi/Introductory-Nuclear-Physics-new-Krane.pdf

[15] Live Chart of Nuclides: nuclear structure and decay data. *Nuclear Data Services* [online]. Austria: IAEA, 2022, 2022 [cit. 2022-01-07]. Available online: https://www-nds.iaea.org/relnsd/vcharthtml/VChartHTML.html

[16] *Frontier Technology Corporation: World's expert in neutron sources* [online]. USA: FTC, 2022 [cit. 2022-01-08]. Available online: https://www.frontier-cf252.com/

[17] CHADWICK, James. The existence of a neutron. *Proceedings of the Royal Society of London. Series A, Containing Papers of a Mathematical and Physical Character* [online]. 1932, **136**(830), 692-708 [cit. 2022-01-09]. ISSN 0950-1207. DOI:10.1098/rspa.1932.0112

[18] *ISO 8529-1:2021: Neutron reference radiations fields - Part 1: Characteristics and methods of production.* 2. 2021, 30 s.

[19] Americium-Beryllium (AmBe) Neutron Sources for Oil Well Logging. *QSA Global* [online]. QSA Global, 2022 [cit. 2022-01-12]. Available online: https://www.qsa-global.com/ambe-neutron-sources-ow

[20] BAGI, János, László LAKOSI a Cong Tam NGUYEN. Neutron producing reactions in PuBe neutron sources. *Nuclear Instruments and Methods in Physics Research Section B: Beam Interactions with Materials and Atoms* [online]. 2016, **366**, 69-76 [cit. 2022-01-08]. ISSN 0168583X. DOI:10.1016/j.nimb.2015.10.004

[21] HOLMES, R.J. Gamma ray and neutron sources. WATT, J.S. *Australian Atomic Energy Commission Research Establishment* [online]. Australia, 1982, s. 123-136 [cit. 2021-12-13]. Available online: https://inis.iaea.org/collection/NCLCollectionStore/_Public/14/792 /14792880.pdf?r=1

[22] Secondary Sources: Double Encapsulated Secondary Source Assemblies (SSAs). *Westinghouse* [online]. Westinghouse Electric Company LLC., 2016 [cit. 2022-01-13]. Available online: https://www.westinghousenuclear.com/Portals/0/flysheets/NFCM-0013_SecondarySources.pdf

[23] VAN DER LEDEN, L. T. *Development of a neutron source model for DEMO and nuclear response analysis of in-vessel components* [online]. 2020 [cit. 2022-01-21]. Available online: https://pure.tue.nl/ws/portalfiles/portal/167947563/0908982_Leden_L.T._ van_der_Master_thesis.pdf. Master thesis.

[24] HAJI EBRAHIMI, E., R. AMROLLAHI, A. SADIGHZADEH, M. TORABI, M. SEDAGHAT, R. SABRI, B. POURSHAHAB a V. DAMIDEH. The Influence of Cathode Voltage and Discharge Current on Neutron Production Rate of Inertial Electrostatic Confinement Fusion (IR-IECF). *Journal of Fusion Energy* [online]. 2013, **32**(1), 62-65 [cit. 2022-01-09]. ISSN 0164-0313. DOI:10.1007/s10894-012-9524-6

[25] IKEDA, Shunsuke, Masahiro OKAMURA, Takeshi KANESUE, et al. Neutron generator based on intense lithium beam driver. *Review of Scientific Instruments* [online]. 2020, **91**(2) [cit. 2022-01-10]. ISSN 0034-6748. DOI:10.1063/1.5128421

[26] Types of accelerators. *Accelerators of society* [online]. TIARA, 2013 [cit. 2022-01-09]. Available online: http://www.accelerators-for-society.org/about-accelerators/index.php?id=21#cockroft

[27] *GANIL-SPIRAL2: Grand Accélérateur National d'Ions Lourds* [online]. France, 2022 [cit. 2022-04-25]. Available online: https://www.ganil-spiral2.eu/

[28] LEDOUX, X., J. C. FOY, J. E. DUCRET, et al. First beams at neutrons for science. *The European Physical Journal A* [online]. 2021, **57**(8) [cit. 2022-01-04]. ISSN 1434-6001. DOI:10.1140/epja/s10050-021-00565-x

[29] FILOVÁ, V. a D. KRÁL. Laserem řízené urychlování částic: Diagnostika a směr budoucího výzkumu. In: *Jaderná energetika v pracích mladé generace - 2019*

[online]. Praha: Česká nukleární společnost, 2020, s. 26-31 [cit. 2022-01-10]. ISBN 978-80-02-02895-6. Available online: https://nuklearnispolecnost.cz/wp-content/uploads/2021/04/FINAL-sbornik_2019.pdf

[30] KE, Jianlin, Chunlei WU, Meng LIU, et al. A compact accelerator-driven deuterium—deuterium neutron source using heavy water jet target. *Nuclear Instruments and Methods in Physics Research Section A: Accelerators, Spectrometers, Detectors and Associated Equipment* [online]. 2021, **997** [cit. 2022-01-10]. ISSN 01689002. DOI:10.1016/j.nima.2021.165165

[31] MINSKY, D.M. a A.J. KREINER. Near threshold 7Li(p,n) 7Be reaction as neutron source for BNCT. *Applied Radiation and Isotopes* [online]. 2015, **106**, 68-71 [cit. 2021-12-27]. ISSN 09698043. Available online: DOI:10.1016/j.apradiso.2015.07.038

[32] STEFANIK, Milan, Eva SIMECKOVA, Pavel BEM, et al. Neutron spectrum determination of p Be reaction for 30 MeV protons using the multi-foil activation technique. *EPJ Web of Conferences* [online]. 2020, **239** [cit. 2022-01-04]. ISSN 2100-014X. DOI:10.1051/epjconf/202023917015

[33] *Nuclear Physics Institute CAS: public research institution* [online]. Řež: CAS [cit. 2022-01-05]. Available online: http://www.ujf.cas.cz/en/

[34] NDLOVU, N.B., P.P. MALEKA a F.D. SMIT. Upgrade of the iThemba LABS Neutron Beam Vault to a Metrology Facility. In: *International Conference on Cyclotrons and their Applications (22nd)* [online]. Geneva, Switzerland: JACoW Publishing, 2020, s. 181-184 [cit. 2022-01-27]. ISBN 978-3-95450-205-9. Available online: DOI:10.18429/JACoW-Cyclotrons2019-TUP012

[35] BAXTER, David V., J. LEUNG, Helmut KAISER, et al. Neutron Moderator Development Research at the Low Energy Neutron Source. *Physics Procedia* [online]. 2012, **26**, 117-123 [cit. 2022-01-06]. ISSN 18753892. DOI:10.1016/j.phpro.2012.03.016

[36] TASAKI, S., T. NAGAE, M. HIROSE, et al. Properties and Possible Applications of Kyoto University Accelerator Based Neutron Source (KUANS). *Physics Procedia* [online]. 2014, **60**, 181-185 [cit. 2022-01-06]. ISSN 18753892. DOI:10.1016/j.phpro.2014.11.026

[37] FERNANDEZ-ALONSO, Felix. *Neutrons at ESS-Bilbao: From Production to Utilisation.* Science and Technology Facilities Council, 2013. ISSN 1358-6254. Report number: RAL-TR-2013-016. Available online:

https://www.researchgate.net/publication/327672298_Neutrons_at_ESS-Bilbao_From_Production_to_Utilisation

[38] ZOU, Yubin, Weiwei WEN, Zhiyu GUO, et al. PKUNIFTY: A neutron imaging facility based on an RFQ accelerator. *Nuclear Instruments and Methods in Physics Research Section A: Accelerators, Spectrometers, Detectors and Associated Equipment* [online]. 2011, **651**(1), 62-66 [cit. 2022-01-06]. ISSN 01689002. DOI:10.1016/j.nima.2011.02.011

[39] WEI, Jie, Huaibi CHEN, Cheng CHENG, et al. The Compact Pulsed Hadron Source: A Design Perspective. *Journal of the Korean Physical Society* [online]. 2010, **56**(6(1), 1928-1936 [cit. 2022-01-04]. ISSN 0374-4884. DOI:10.3938/jkps.56.1928

[40] KOBAYASHI, Tomohiro, Shota IKEDA, Yoshie OTAKE, Yujiro IKEDA a Noriyosu HAYASHIZAKI. Completion of a new accelerator-driven compact neutron source prototype RANS-II for on-site use. *Nuclear Instruments and Methods in Physics Research Section A: Accelerators, Spectrometers, Detectors and Associated Equipment* [online]. 2021, **994** [cit. 2022-01-06]. ISSN 01689002. DOI:10.1016/j.nima.2021.165091

[41] PORRA, Liisa, Tiina SEPPÄLÄ, Lauri WENDLAND, et al. Accelerator-based boron neutron capture therapy facility at the Helsinki University Hospital. *Acta Oncologica* [online]. , 1-5 [cit. 2022-01-28]. ISSN 0284-186X. DOI:10.1080/0284186X.2021.1979646

[42] BISELLO, D., E. FAGOTTI, J. ESPOSITO, et al. LINUS, the Integrated LNL Neutron Source facility. *Journal of Physics: Conference Series* [online]. 2018, **1021** [cit. 2022-01-11]. ISSN 1742-6588. DOI:10.1088/1742-6596/1021/1/012010

[43] SILVERMAN, Ido, Alex ARENSHTAM, Dan BERKOVITS, et al. *Scientific opportunities at SARAF with a liquid lithium jet target neutron source* [online]. 2018, , 020002- [cit. 2022-01-05]. DOI:10.1063/1.5035515

[44] GUTBERLET, T., U. RÜCKER, E. MAUERHOFER, et al. Sustainable neutrons for today and tomorrow-The Jülich High Brilliance neutron Source project. *Neutron News* [online]. 2020, **31**(2-4), 37-43 [cit. 2022-01-04]. ISSN 1044-8632. DOI:10.1080/10448632.2020.1819132

[45] THULLIEZ, Loïc, Alain LETOURNEAU, Jérôme SCHWINDLING, et al. First steps toward the development of SONATE, a Compact Accelerator driven Neutron Source. *EPJ Web of Conferences* [online]. 2020, **239** [cit. 2022-01-03]. ISSN 2100-014X. DOI:10.1051/epjconf/202023917011

[46] MAUERHOFER, Eric, et al. *NOVA ERA (Neutrons Obtained Via Accelerator for Education and Research Activities): Conceptual Design Report* [online]. Verlag Jülich: Forschungszentrum Jülich GmbH Zentralbibliothek, 2017, 68 s. [cit. 2022-01-05]. ISBN 978-3-95806-280-1. Available online: https://www.fz-juelich.de/SharedDocs/Downloads/JCNS/JCNS-2/EN/Conceptual-Design.pdf?___blob=publicationFile

[47] BATYGIN, Yuri K., Eric J. PITCHER, Helmut KAISER, et al. Advancement of LANSCE accelerator facility as a 1-MW Fusion Prototypic Neutron Source. *Nuclear Instruments and Methods in Physics Research Section A: Accelerators, Spectrometers, Detectors and Associated Equipment* [online]. 2020, **960**, 117-123 [cit. 2022-01-06]. ISSN 01689002. DOI:10.1016/j.nima.2020.163569

[48] *ISIS Neutron and Muon Source* [online]. UK: STFC, 2022 [cit. 2022-01-04]. Available online: https://www.isis.stfc.ac.uk/

[49] GEUE, Thomas, Fanni JURANYI, Christof NIEDERMAYER, et al. SINQ-Performance of the New Neutron Delivery System. *Neutron News* [online]. 2021, **32**(2), 37-43 [cit. 2021-12-31]. ISSN 1044-8632. DOI:10.1080/10448632.2021.1916267

[50] GUNSING, F., U. ABBONDANNO, G. AERTS, et al. *Nuclear Instruments and Methods in Physics Research Section B: Beam Interactions with Materials and Atoms* [online]. 2007, **261**(1-2) [cit. 2022-01-04]. ISSN 0168583X. DOI:10.1016/j.nimb.2007.03.096

[51] *Oak Ridge National Laboratory: Neutron Sciences* [online]. USA: ORNL [cit. 2022-01-04]. Available online: https://neutrons.ornl.gov/

[52] TAKADA, Hiroshi a Katsuhiro HAGA. Recent Status of the Pulsed Spallation Neutron Source at J-PARC. *Proceedings of the 14th International Workshop on Spallation Materials Technology* [online]. Journal of the Physical Society of Japan, 2020, 2020-02-06, , - [cit. 2022-01-05]. ISBN 4-89027-138-4. DOI:10.7566/JPSCP.28.081003

[53] TANG, Jing-Yu, Qi AN, Jiang-Bo BAI, et al. Back-n white neutron source at CSNS and its applications. *Nuclear Science and Techniques* [online]. 2021,

32(1), 117-123 [cit. 2022-01-06]. ISSN 1001-8042. DOI:10.1007/s41365-021-00846-6

[54] GAROBY, Roland, A VERGARA, H DANARED, et al. The European Spallation Source Design. *Physica Scripta* [online]. 2018, **93**(1) [cit. 2021-12-30]. ISSN 0031-8949. DOI:10.1088/1402-4896/aa9bff

[55] *BrightnESS²* [online]. Sweden: ESS [cit. 2022-01-03]. Available online: https://brightness.esss.se/

[56] OLACEL, Adina, Catalin BORCEA, Marian BOROMIZA, et al. Neutron inelastic cross section measurements on 58,60 Ni. *EPJ Web of Conferences* [online]. 2020, **239** [cit. 2022-01-04]. ISSN 2100-014X. DOI:10.1051/epjconf/202023901040

[57] GRANADA, J. R., R. E. MAYER, J. DAWIDOWSKI, J. R. SANTISTE-BAN, F. CANTARGI, J. J. BLOSTEIN, L. A. RODRÍGUEZ PALOMINO a A. TARTAGLIONE. The sciences and applications of the Electron LINAC-driven neutron source in Argentina. *The European Physical Journal Plus* [online]. 2016, **131**(6) [cit. 2022-01-04]. ISSN 2190-5444. DOI:10.1140/epjp/i2016-16216-2

[58] HARA, Kaoru Y, et al. HUNS upgrade. Simulation of the beam profile for a thermal neutron source in HUNS-2. *Proceedings of the 2019 Symposium on Nuclear Data, November 28-30, 2019* [online]. JAEA, 2020, , 165-170 [cit. 2022-01-06]. Report Number: JAEA-CONF–2020-001. DOI:10.11484/jaea-conf-2020-001

[59] SHVETSOV, Valery. Neutron Sources at the Frank Laboratory of Neutron Physics of the Joint Institute for Nuclear Research. *Quantum Beam Science* [online]. 2017, **1**(1) [cit. 2022-01-04]. ISSN 2412-382X. DOI:10.3390/qubs1010006

[60] BEYER, R., E. BIRGERSSON, Z. ELEKES, et al. Characterization of the neutron beam at nELBE. *Nuclear Instruments and Methods in Physics Research Section A: Accelerators, Spectrometers, Detectors and Associated Equipment* [online]. 2013, **723**, 151-162 [cit. 2022-01-04]. ISSN 01689002. DOI:10.1016/j.nima.2013.05.010

[61] SEKI, Y., J.M. BEREDER a M. UESAKA. Development of Mobile Neutron Sources Driven by X-Band Electron Linacs for Infrastructure Maintenance and Nuclear Security. In: *IPAC2016, Busan, Korea* [online]. Geneva, Switzerland: JACoW [cit. 2022-01-28]. ISBN 978-3-95450-147-2. Available online: DOI:10.18429/JACoW-IPAC2016-WEPMY041

[62] Research Reactor Database. *International Atomic Energy Agency* [online]. Austria: IAEA [cit. 2022-01-11]. Available online: https://nucleus.iaea.org/rrdb/#/home

[63] BARANYAI, Rózsa F., et al. *Budapest Research Reactor: 60 Years of Research & Innovation* [online]. In: . Budapest, 2019, s. 18 [cit. 2021-12-30]. Available online: https://www.bnc.hu/sites/default/files/BRR_60_Web_preview_190328.pdf

[64] *The Institute for Solid State Physics the University of Tokyo* [online]. Japan: ISSP, 2021 [cit. 2022-01-11]. Available online: http://www.issp.u-tokyo.ac.jp/

[65] CHANDLER, D., B. R. BETZLER, D. H. COOK, M. MARGULIS a P. BLAISE. REACTOR PERFORMANCE IMPROVEMENT OPTIONS TO SUSTAIN HIGH FLUX ISOTOPE REACTOR LEADERSHIP INTO THE FUTURE*. *EPJ Web of Conferences* [online]. 2021, **247** [cit. 2022-01-06]. ISSN 2100-014X. DOI:10.1051/epjconf/202124708016

[66] *Institut Laue-Langevin: Neutrons for Society* [online]. Grenoble, France: Institut Laue-Langevin [cit. 2022-01-04]. Available online: https://www.ill.eu/

[67] KRZYSZTOSZEK, Grzegorz a C. GALLÉ. The Characteristics and Irradiation Capabilities of MARIA Research Reactor in NCBJ Świerk. *EPJ Web of Conferences* [online]. 2016, **115** [cit. 2022-01-03]. ISSN 2100-014X. DOI:10.1051/epjconf/201611501004

[68] *Forschungs-Neutronenquelle Heinz Maier-Leibnitz (FRM II)* [online]. Germany: Technische Universität München [cit. 2021-12-31]. Available online: https://www.frm2.tum.de/en/frm2/home/

[69] The Garching research reactor is scheduled to start up again in 2022 — no new fuel. *Market Research Telecast* [online]. MRT, 25.09.2021 [cit. 2022-01-11]. Available online: https://marketresearchtelecast.com/the-garching-research-reactor-is-scheduled-to-start-up-again-in-2022-no-new-fuel/164301

[70] *ANSTO* [online]. Australia: ANSTO, 2022 [cit. 2022-01-05]. Available online: https://www.ansto.gov.au/

[71] *Petersburg Nuclear Physics Institute* [online]. Russia: PNPI, 2022 [cit. 2022-01-06]. Available online: http://www.pnpi.spb.ru/en/

[72] *Comisión Nacional de Energía Atómica* [online]. Argentina unida [cit. 2022-01-11]. Available online: https://www.argentina.gob.ar/cnea

[73] MEYERS, Robert A., ed. *Encyclopedia of Physical Science and Technology* [online]. 3. California, USA: Academic Press, 2001, 15453 s. [cit. 2021-12-21]. ISBN 978-0-12-227410-7. Available online: https://www.sciencedirect.com/referencework/9780122274107/encyclopedia-of-physical-science-and-technology

[74] CACUCI, D. G. *Handbook of Nuclear Engineering* [online]. Boston: Springer US, 2010 [cit. 2021-12-21]. ISBN 978-0-387-98130-7. Available online: DOI:10.1007/978-0-387-98149-9

[75] REILLY, D. a N. ENSSLIN. *Passive nondestructive assay of nuclear materials* [online]. United States: Nuclear REgulatory Commision, 1991, 700 s. [cit. 2021-12-21]. ISBN 0-16-032724-5. LA-UR-90-732. Available online: https://www.lanl.gov/orgs/n/n1/FMTTD/neut_mc/pdfs/LA_UR_90_0732.pdf

[76] BROWN, D.A., M.B. CHADWICK, R. CAPOTE, et al. ENDF/B-VIII.0: The 8 th Major Release of the Nuclear Reaction Data Library with CIELO-project Cross Sections, New Standards and Thermal Scattering Data. *Nuclear Data Sheets* [online]. 2018, **148**, 1-142 [cit. 2022-05-19]. ISSN 00903752. DOI:10.1016/j.nds.2018.02.001

[77] GILMORE, Gordon R. *Practical Gamma-Ray Spectrometry* [online]. 2. John Wiley Sons, 2008 [cit. 2022-05-13]. ISBN 9780470861981. DOI:10.1002/9780470861981

[78] EXFOR Statistics. *IAEA Nuclear Data Services* [online]. Austria, 2022 [cit. 2022-04-24]. Available online: https://www-nds.iaea.org/exfor/x4stat/exfor_stat.htm

[79] ALI, Muhammad, Aziz Ahmed QURESHI, Abdul WAHEED, Muzahir Ali BALOCH, Hamza QAYYUM, Muhammad TUFAIL a Hameed Ahmed KHAN. Assessment of radiological hazard of NORM in Margalla Hills limestone, Pakistan. *Environmental Monitoring and Assessment* [online]. 2012, **184**(8), 4623-4634 [cit. 2022-05-19]. ISSN 0167-6369. Available online:: doi:10.1007/s10661-011-2290-5

[80] FRÁNA, J. Program DEIMOS32 for gamma-ray spectra evaluation. *Journal of Radioanalytical and Nuclear Chemistry* [online]. 2003, **257**(3), 583-587 [cit. 2022-05-12]. ISSN 0236-5731. DOI:10.1023/A:1025448800782

[81] CHUDOBA, Petr. *Study of reaction cross-sections important for advanced nuclear systems* [online]. Prague, 2018 [cit. 2022-05-24]. Available online:: http://ojs.ujf.cas.cz/ wagner/transmutace/diplomky/chudoba_PhD/thesis_final_Chudoba.pdf. Doctoral Thesis. Nuclear Physics Institute of the CAS p.r.i. Supervisor Vladimír Wagner.

[82] SUDAR, S. *'TrueCoinc' software utility for calculation of the true coincidence correction* [online]. In: . Austria: International Atomic Energy Agency, 2002, s. 37-48 [cit. 2022-05-19]. ISSN 1011-4289. Available online:: https://inis.iaea.org/search/search.aspx?orig_q=RN:33017174

[83] SVOBODA, Ondřej. *Experimental Study of Neutron Production and Transport for ADTT* [online]. Prague, 2011 [cit. 2022-05-19]. Available online: http://ojs.ujf.cas.cz/ wagner/transmutace/diplomky/PHD_Svoboda.pdf. Dissertation Thesis. Czech Technical University in Prague. Supervisor Vladimír Wagner.

[84] SIMECKOVA, E., P. BEM, V. BURJAN, et al. The Measurement of Neutron Activation Cross Section of 59Co Below 36 MeV. *Journal of the Korean Physical Society* [online]. 2011, **59**(2(3), 1801-1804 [cit. 2022-05-19]. ISSN 0374-4884. DOI:10.3938/jkps.59.1801

[85] Král D. et al. Software pro vyhodnocení měřeného spektra neutronů. *Ústav elektroenergetiky* [online]. 2022 [cit. 2022-05-12]. Available online: https://www.ueen.fekt.vut.cz/software-pro-vyhodnoceni-mereneho-spektra-neutronu

[86] IWAMOTO, Osamu, Nobuyuki IWAMOTO, Keiichi SHIBATA, et al. Status of JENDL. *EPJ Web of Conferences* [online]. 2020, **239** [cit. 2022-05-19]. ISSN 2100-014X. DOI :10.1051/epjconf/202023909002

[87] KONING, A.J., D. ROCHMAN, J.-Ch. SUBLET, N. DZYSIUK, M. FLEMING a S. VAN DER MARCK. TENDL: Complete Nuclear Data Library for Innovative Nuclear Science and Technology. *Nuclear Data Sheets* [online]. 2019, **155**, 1-55 [cit. 2022-05-19]. ISSN 00903752. DOI:10.1016/j.nds.2019.01.002

[88] OTUKA, N., E. DUPONT, V. SEMKOVA, et al. Towards a More Complete and Accurate Experimental Nuclear Reaction Data Library (EXFOR): International Collaboration Between Nuclear Reaction Data Centres (NRDC). *Nuclear Data Sheets* [online]. 2014, **120**, 272-276 [cit. 2022-05-19]. ISSN 00903752. DOI:10.1016/j.nds.2014.07.065

Symbols and abbreviations

AmB   Americium-Boron

AmBe   Americium-Beryllium

ANDA   Active NonDestructive Analysis

ANSTO   Australian Nuclear Science and Technology Organisation

BNCT   Boron Neutron Capture Therapy

BRR   Budapest Research Reactor

CAEP   China Academy of Engineering Physics

CANS   Compact Accelerator-driven Neutron Source

CERN   Conseil Européen pour la Recherche Nucléaire

CPHS   Compact Pulsed Hadron Source

CSNS   China Spallation Neutron Source

DC   Direct Current

DD   Deuterium-Deuterium

DT   Deuterium-Tritium

ELBE   Electron Linear accelerator with high Brilliance and low Emittance

ENDF   Evaluated Nuclear Data File

ESS   European Spallation Source

ESSB   European Spallation Source Bilbao

EXFOR   EXchange FORmat for experimental numerical nuclear reaction data

FPNS   Fusion Prototypic Neutron Source

FRM-II   Forschungsreaktor Munchen

GELINA   Geel Electron LINear Accelerator

HBN   High Brilliance Neutron source

HFIR   High Flux Isotope Reactor

HFR   High Flux Reactor

HEU   High Enriched Uranium

HPGe   High Purity Germanium

HUNS   Hokkaido University Neutron Source

IAEA   International Atomic Energy Agency

IEC   Inertial Electrostatic Confinement

ILL   Institute Laue-Langevin

INC   Intra-Nuclear Cascade

IREN   Intense REsonance Neutron source

ISO   International Organization for Standardization

J-PARC   Japan Proton Accelerator Research Complex

JAEA   Japan Atomic Energy Agency

JEFF   Joint Evaluated Fission and Fusion File

JINR   Joined Institute for Nuclear Research

LABS   Laboratory for Accelerator-Based Sciences

LEU   Low Enriched Uranium

LENS   Low Energy Neutron Source

linac   Linear accelerator

LINUS   Integrated LNL Neutron Source

LNL   Laboratori Nazionali di Legnaro

LANSCE   Los Alamos Neutron Science Center

KUANS   Kyoto University Accelerator-driven Neutron Source

n_TOF   Neutron Time-of-Flight facility

NASA   National Aeronautics and Space Administration

nELBE	neutron source at Electron Linear accelerator with high Brilliance and low Emittance
NFS	Neutrons For Science
PGNAA	Prompt Gamma Neutron Activation Analysis
OPAL	Open Pool Australian Lightwater reactor
ORNL	Oak Ridge National Laboratory
PINS	Portable Isotopic Neutron Spectroscopy System
PKUNIFTY	PeKing University Neutron Imaging FaciliTY
PSI	Paul Scherrer Institute
PuBe	Plutonium-Beryllium
RANS	RIKEN Accelerator-driven Neutron Source
RFI	Radio Frequency Induction
Σ	macroscopic cross-section
σ	microscopic cross-section
SARAF	Soreq Applied Research Accelerator Facility
SbBe	Antimony-Beryllium
SINQ	Swiss Spallation Neutron Source
SNS	Spallation Neutron Source
TOF	Time-of-Flight
TT	Tritium-Tritium